Structural Health Monitoring of Composite Materials with FBG Sensors: Damage Detection and Remaining Useful Life Prediction

by

Talha Boz

Submitted to
the Graduate School of Engineering and Natural Sciences
in partial fulfillment of
the requirements for the degree of
Master of Science

SABANCI UNIVERSITY

September 2012

Structural Health Monitoring of Composite Materials with FBG Sensors: Damage Detection and Remaining Useful Life Prediction

Talha Boz

ME, M.Sc. Thesis, 2012

Thesis Supervisor: Assoc. Prof. Dr. Mehmet Yildiz

Keywords: structural health monitoring (SHM), fiber Bragg grating (FBG) sensor, damage detection, resin transfer molding (RTM), remaining useful life (RUL) prediction.

Abstract

Advanced composites are widely employed in load bearing structures due to their high strength-to-weight ratios, stiffness, corrosion resistance and fatigue performance. Monitoring the manufacturing process and detecting the damage during service are rather troublesome. In this study, practicality and feasibility of fiber optic based sensors are evaluated for monitoring the state or the structural health of the composite materials from manufacturing phase to service phase continuously. 2D and 3D composite structures were designed and manufactured by resin transfer molding (RTM) method. A novel ingress/egress technique is utilized to embed the fiber optic sensors. The capabilities of flow and cure monitoring of fiber Bragg grating (FBG) sensors are presented. The strain and the temperature sensitivity of the embedded FBG sensors was calculated. Following the calculation of the sensitivities, a manufactured composite with embedded FBG sensor is subjected to cantilever beam experiments. To be able to show that the FBG sensor is capable of detecting damage formation in composites, the composite plate was drilled to create artificial defects of different size. The wavelength shift of the FBG was monitored as a function of the size of the hole and wavelength measurements are compared with those of sound structure to conclude on the health of the structure. Technique for prediction of remaining useful life (RUL) of composite materials with embedded FBG sensors is demonstrated and fatigue testing of composite materials are performed to verify this technique.

FBG Sensörler ile Kompozit Malzemelerin Yapısal Sağlık Gözetimi: Hasar Tespiti ve Kalan Kullanılabilir Ömür Tahmin Etme

Talha Boz

ME, M.Sc. Tez, 2012

Tez Danışmanı: Doç. Dr. Mehmet Yıldız

Anahtar kelimeler: yapısal sağlık gözetimi (SHM), fiber Bragg ızgara (FBG) sensörü, hasar bulma, reçine iletim kalıplama (RTM), kalan ömür tahmin etme (RUL)

Özet

İleri kompozit yapılar yüksek ağırlık-güç oranları, sertlik değerleri, aşınma dirençleri ve yorulma performansları nedeniyle yük taşıyan yapılarda çoğunlukla kullanılmaktadırlar. Kompozit yapılarda üretim sürecini gözlemlemek ve kullanım sırasında hasar tespiti yapmak zordur. Bu çalışmada, fiber optik tabanlı sensörlerin kompozit malzemelerin yapısal sağlığını ve durumunu üretim sürecinden malzemenin son kullanımına kadar sürekli olarak gözlemleme kabiliyeti uygulanabilirlik ve kullanışlılık açısından değerlendirilmiştir. 2 ve 3 boyutlu kompozit yapılar tasarlanmış ve reçine geçiş kalıplaması (RTM) yöntemi ile üretilmişlerdir. Fiber optik sensörleri yapı içine gömmek için yeni geliştirilen giriş/çıkış yöntemi kullanılmıştır. Fiber Bragg Izgara (FBG) sensörlerinin akış ve kürleşmeyi gözlemleme kabiliyetleri gösterilmiştir. Gömülü FBG sensörlerin gerinim ve sıcaklık hassasiyetleri hesaplanmıştır. Gömülü FBG sensör bulunduran bir kompozit plaka ile konsol kiriş deneyleri yapılmıştır. FBG sensörün kompozit üzerindeki hasarı tespit etme kapasitesini göstermek için kompozit plaka üzerinde farklı boyutlarda yapay hasarlar oluşturulmuştur. FBG sensörün dalga boyu değişimi grafiği deliğin boyutuna göre çizdirilmiş ve hasarlı yapı ile yapılan dalga boyu ölçümleri yapının sağlığı hakkında yorum yapabilmek için hasarsız yapı ile yapılan ölçümlerle karşılaştırılmıştır. Kalan kullanılabilir ömür (RUL) tahmin etme tekniği, içerisinde FBG sensör barındıran kompozit malzemeler için geliştirilmiş ve bu tekniğin uygulaması üretilen kompozit malzemelerin yorulma deneyleri ile yapılmıştır.

To my wife Edibe and my son Furkan...

Acknowledgements

I would like to thank to

Professor Mehmet Yildiz, as my adviser he provided professional and personal guidance and support throughout every aspect of this work.

My reading committee members, Professors **Mustafa Unel, Ali Kosar, Burc Misirlioglu, Cem Ozturk and Bahattin Koc** for their helpful comments on the draft of this thesis.

ITU ROTAM and **Professor Halit Turkmen** for letting me use their facillities.

TUBITAK BIDEB for funding my graduate education for 2 years and **TUBITAK** for supporting our project, project number of 108M229.

My collegues at our laboratory, Fazli Fatih Melemez, Dr. Pandian Chelliah, Dr. Casey Keulen, Ataman Deniz and Cagatay Yilmaz for their helps and guidance during the course of my thesis.

My family for their unending love and support from the beginning of my life.

My wife Edibe for her patience, encouragement and never ending support through my graduate education.

My son Furkan who supported and encouraged me by just smiling at me.

Contents

List of Figures

List of Tables

Chapter 1

Introduction

1.1 Motivation

Composite materials have been utilized in load bearing structures such as airplanes, wind turbines, pressure vessels as an alternative to metallic materials due to their high strength-to-weight ratios, stiffness, corrosion resistance and fatigue performance [33, 40, 44]. The life of a smart composite material starts with the concept and design phase where the assessment of requirements and constraints is conducted, and the properties expected of the composite material is determined. This phase is followed by the manufacturing phase in which the composite material is produced with a chosen method in light of the design parameters. Evidently, service phase is the last step where the composite is utilized in a structure. A life of a smart composite is represented schematically in Figure 1.1.

Although composite materials offer superb material properties, manufacturing of composite materials and their assessment against damage during their service are rather troublesome. One of the greatest challenges with the manufacturing phase is related to the curing of the resin since it is not an easy task to determine if the curing process is successfully completed or not. Another challenge is related to successful or full impregnation of fiber reinforcement by the injected resin. Traditional process monitoring methods provide information on a global scale and

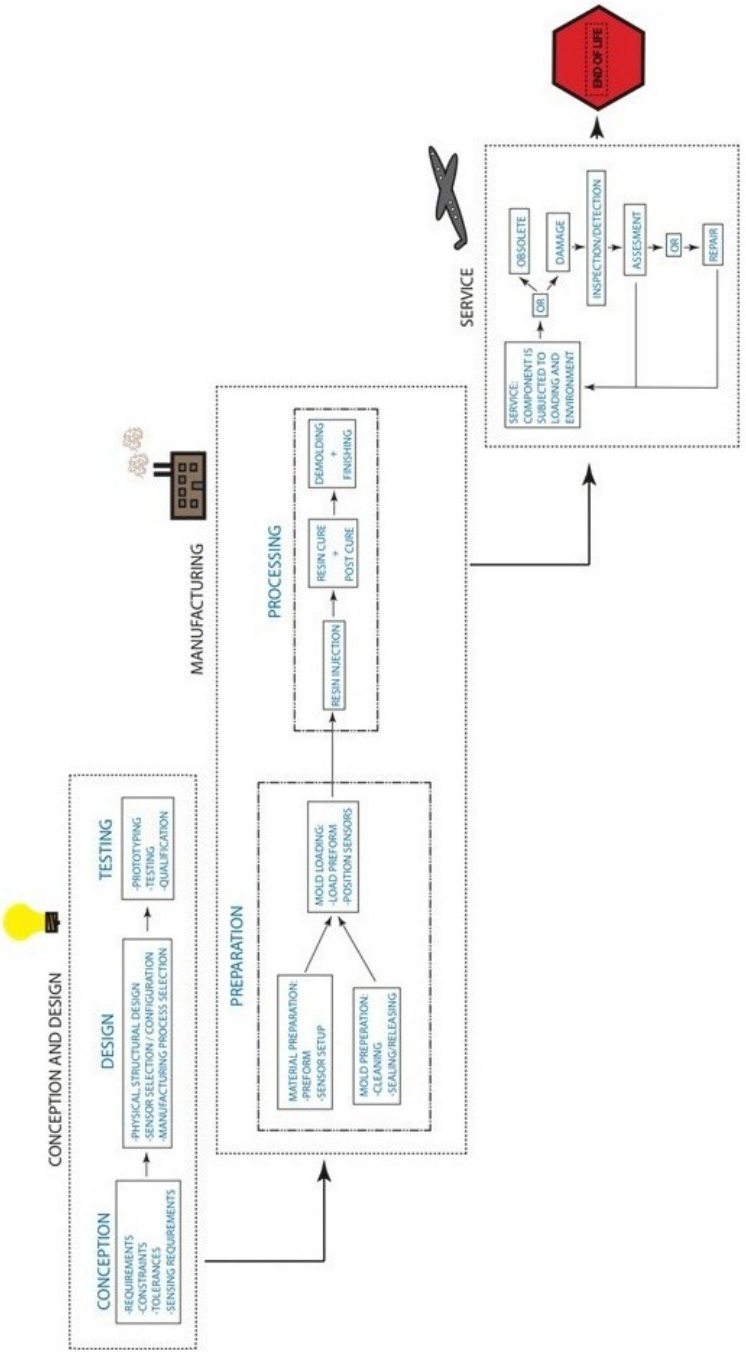

FIGURE 1.1: Life of a smart composite

cannot detect the local regions which are not saturated with resin. If these resin deficient or unsaturated regions are not detected, they can easily endanger the life of the composite material hence resulting in the occurrence of catastrophic failures. The challenge associated with the service phase is due to need for continuous monitoring of the health of the composite structure, which is referred to

as the Structural Health Monitoring (SHM). Although damage detection in composite materials is performed with non-destructive evaluation methods such as X-ray, ultrasonic and thermal imaging, among many others, these non-destructive testing (NDT) methods do not provide any real time information or data about the conditions of the composite material under the service. Hence, without the availability of SHM systems integrated with composite materials, the composite structures need to be taken out of service and have to be inspected periodically to ensure their well-being and reliability. Despite the fact that composite materials are periodically evaluated or inspected at wisely chosen time intervals to circumvent any unexpected sudden failure, they may fail in service before the next periodic evaluation.

Moreover, NDTs can be rather time consuming and expensive compared to continuous structural health monitoring with embedded fiber optic sensors. Due to the size of the test machines and the location of the part that requires inspection, the structure might have to be disassembled which is the case for airplanes. In the case of an airplane or a ship, the inspection of a large structural members will take time, which holds the carrier out of the service. After disassembling the structure and testing the parts in detail, the reassembly of the structure may create some other unforeseen problems. Additionally, unlike metallic structures which can be put together with rivets, bolts, and welding, the composite materials may not easily use the traditional assembly methodologies or techniques. All these aforementioned difficulties in relation to periodic inspection or evaluation of composite structures indicate that there should be an alternative approach whereby the health of the composite structure can be monitored continuously in real time without the need of any periodic disassembly and reassembly processes.

In light of above provided discussion, the motivation behind this work is to evaluate practicality and the feasibility of fiber optic based sensors for monitoring the state or the structural health of the composite materials from cradle to grave continuously, or from manufacturing phase to service phase. In regard to the motivation, within the scope of the current MSc study, three goals were set. The first one was to design and manufacture advanced 2D and 3D composite structures by

using resin transfer molding (RTM) method. The second one was to embed fiber Bragg grating (FBG) sensors into composite structures with the purpose of monitoring the manufacturing process. Once embedded into composite structures, the third goal is to asses FBG sensors for damage detection and remaining useful life prediction of composite material. The embedded sensors acquire data from the composite structure in real time and detect the presence of any damage. Once the presence of damage or damages is detected, the conventional NDT methods can be utilized to localize the damage or defects in size or shape. Toward this end, the SHM approach does not aim to replace NDT methods, on the contrary, they complete the SHM process. In conclusion, the SHM approach eliminates the necessity of periodic inspection hence reducing the inspection and out of service time of the structure through providing condition based inspection or maintenance.

1.2 Outline of the thesis

The rest of this thesis is organized as follow. Chapter 2 gives brief background information on composites structures, structural health monitoring concept, fiber optic sensors and remaining life prediction. In Chapter 3, composite manufacturing method utilized, namely, resin transfer molding technique and specimen fabrications are described along with method developed and utilized for embedding fiber optic sensors into composite materials. Subsequently, the verification of the embedded FBG sensors is also included. In Chapter 4, experiments conducted for damage detection in composite materials with embedded fiber optic sensors are presented. In Chapter 5, fatigue monitoring of composite materials and results from the remaining useful life prediction from fiber optic sensors are demonstrated. The present work is concluded with a final remark in Chapter 6.

Chapter 2

Background

2.1 Introduction

This chapter provides a reader with relatively comprehensive information on fiber optics, fiber optic sensors, the application of fiber optic sensors to the structural health monitoring and remaining useful life prediction of composite materials.

2.2 Fiber optics

Optical fibers or fiber optics are made of glass which has a nearly similar diameter of a human hair. The light travels inside the region referred to as core which is made of very pure glass around $1 - 5\mu m$ in diameter. The core is surrounded by another glass region called cladding which is around $125\mu m$ in diameter. This region keeps the light inside the core region by having a lower refractive index than the core region. As the light hits the boundary between cladding and core, light reflects from the boundary hence ensuring that light travels inside the core region. To protect the fiber optics, a layer of plastic (generally polyimide or acrylate) is wrapped around the cladding and core. The diameter of this layer is usually $250\mu m$. Depending on where the fiber optics will be used, there might be another

protection medium so that any kind of bending will not break the fiber such as in communication industry.

Fiber optics were first employed with the aim of conveying light and images for medical applications. They were designed to enter the body, travel a sufficient distance into the body and obtain data while being as unobtrusive as possible. Once their potential for carrying data was proven by the medical field optical fibers were used extensively by the communications industry beginning in the 1960s [25]. Recently fiber optics have been employed in engineered structures from bridges and buildings to composite materials by being embedded into the structure thereby enabling data acquisition from inside of the structure as in the case of their original usage in medical applications. As optical fiber is quite small in diameter, it has insignificant effect on the integrity and the material properties of the host material or structure [65]. Embedding fiber optics into the composite materials allows for measuring external effects on the structure such as temperature, strain, among many others.

2.3 Fiber optic sensors

Several different types of fiber optic sensors exist today. Each type of sensors has its advantages and disadvantages depending on the application considered. Fiber optic sensors can be divided into two main categories extrinsic or intrinsic [65]. In extrinsic sensors, light leaves the fiber and it is modulated by another device apart from the fiber. On the other hand, in intrinsic sensors, light is kept inside the fiber and modulation of light occurs inside the fiber. The sensors discussed below are interferomatic type fiber optic sensors which are generally used in relation to composite materials and do not cover all different fiber optic sensors available in today's technology.

2.3.1 Extrinsic fabry-perot interferometer based sensors

In Extrinsic Fabry-Perot interferometer sensors (EFPI), two bare fibers are bonded inside a hollow tube with a gap between them as shown in Figure 2.1.. The ends of the fibers create reflection surfaces to the transmitted light. Light is launched from one end of the fibers. When the light reaches to the gap between two fibers, it bounces back and forth inside the gap. Although most of the wavelengths cancels each out, there are some wavelengths that resonate inside the gap. Those wavelengths forming constructive interference are transmitted through the fiber that light was launched. For resonance to occur, an integral number, N of wavelengths, λ should be equal to the round trip distance in the region, $2L$ as formulated in Eq. 2.1 [25]:

$$2L = \frac{N\lambda}{n} \tag{2.1}$$

where n is the refractive index of the material between the surfaces. The width of the gap can be calculated by the measurement of the interference pattern changes. Strain, temperature and pressure change can be measured using the change in the width of the gap between two fibers.

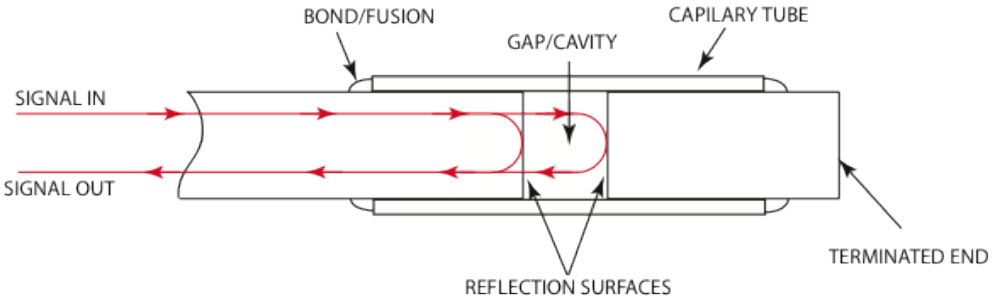

FIGURE 2.1: Schematic of EFPI sensor

2.3.2 Michelson interferometer

A Michelson interferometer is the most common configuration for interferometry. Essentially a light beam is split in two then recombined to create an interference pattern. Each beam travels down a different path, for example through a different

material or path length. The interference pattern can be used to deduce characteristics based on the speed of light through the two paths giving information such as strain, temperature or refractive index.

2.3.3 Fluorescence based sensors

Fluorescence based sensors are especially effective for measuring chemical properties of materials such as viscosity, water vapor content and the degree of cure in polymers [65]. Fluorescent material is applied to one part of the fiber. Then the light is sent toward the fluorescent region and the time rate of decay or spectral content is measured.

2.3.4 Etched fiber sensors

Etched fiber sensor (EFS) is easy and inexpensive to manufacture in a laboratory environment. At a given region of the bare fiber, the cladding is etched chemically to expose the core to the surrounding in question as shown in Figure 2.2. Exposing the core to the outer environment results in change in the intensity of the light because when light reaches the etched region small portion of the light escapes off the fiber optic [25]. The amount of light escaped from the fiber depends on the refractive index of the surroundings in the near vicinity of the etched section. The operation principle of etched fiber sensor for process monitoring (curing, and resin arrival or flow front) is simple. Light is launched from one end and the other end is connected to a optical power meter which measures the light intensity. For example, when the polymeric resin makes contact with the sensor, there is a sudden, sustained drop in the transmitted light intensity [38, 33, 75].

2.3.5 Fiber Bragg grating (FBG) sensors

Fiber Bragg Grating sensors, commonly known as FBG sensors, are the most widely used fiber optics sensors in relation to composite materials in literature.

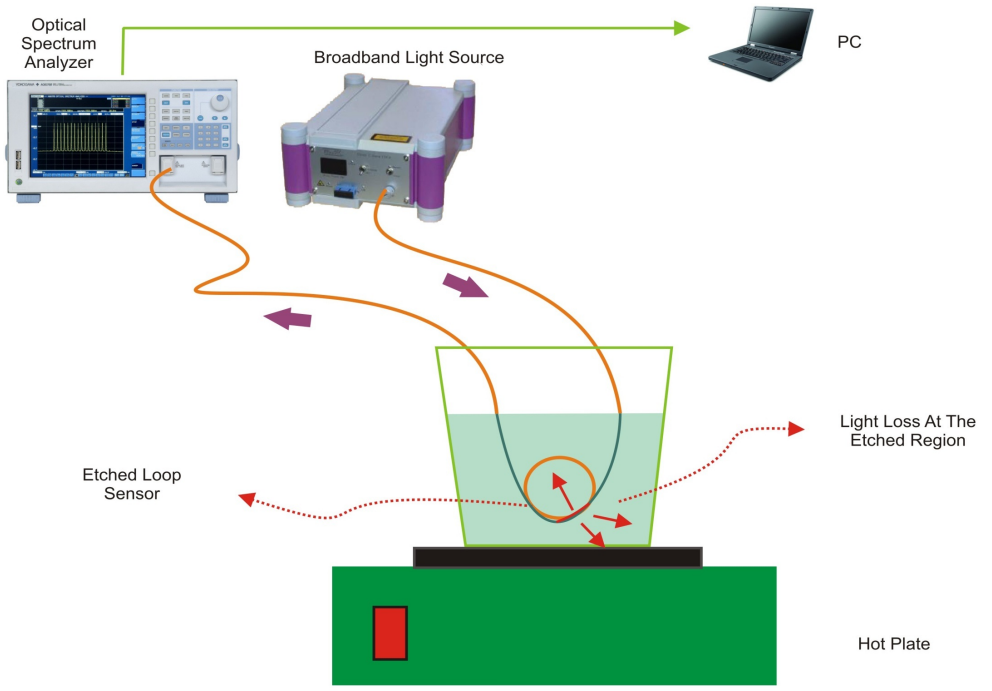

FIGURE 2.2: Experimental setup using etched fiber sensor to measure refractive index

Their compact nature, capacity of multiplexing in large quantities on a single fiber and sensitivity made it possible to be used in different research fields. They were first demonstrated by Hill in 1978 [26] and have been used to measure properties such as displacement, strain, temperature, pressure, humidity and radiation dose among others [13]. Multiplexing ability in a single fiber reduces the ingress and egress points when it is embedded into a structure and makes it possible to create a sensor network that senses spatially distributed strain and temperature data continuously.

An FBG sensor is a segment of a single mode optical fiber inside the core region where the refractive index of this segment is changed periodically in the axial direction of the fiber by means of exposing the region of the interest to a ultraviolet laser [52]. This grating segment acts like an optical filter by reflecting a particular wavelength. The reflected wavelength of the propagating light through the fiber core depends on the grating pitch (spacing between the refractive index variations). The periodic modulation of the refractive index at the grating location will scatter the light traveling inside the fiber core. Out of phase scattered waves will form

destructive interference thereby canceling each other while in phase light waves will add up constructively forming a back-reflected spectrum with a center wavelength known as the Bragg wavelength. If an FBG sensor is exposed to strain or temperature change, the Bragg wavelength of the reflected spectrum shifts hence enabling one to measure this external effects. Figure 2.3 illustrates an FBG sensor.

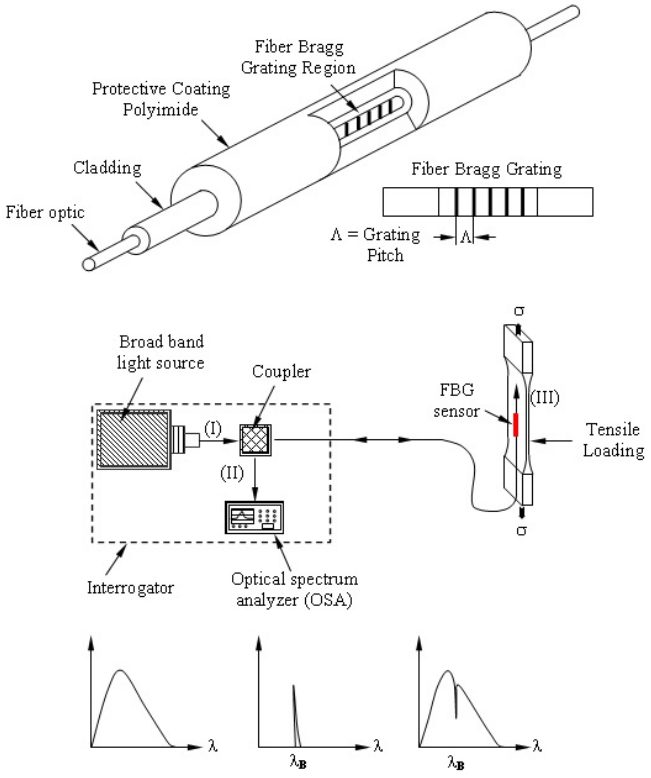

FIGURE 2.3: Illustration of an FBG sensor

The Bragg wavelength satisfies the Bragg condition as Eq. 2.2 [52]:

$$\lambda_b = 2n\Lambda \tag{2.2}$$

where λ_B is the back-reflected Bragg wavelength, n is the average refractive index of the fiber core and Λ is the spacing between gratings. Both the refractive index and the spacing between the gratings are functions of strain and temperature. The spacing of the periodic refractive index modulation and the refractive index are a function of strain and temperature. If an FBG sensor is under a mechanical or thermal load (temperature variation), the spacing between the gratings

and average refractive index will change due to the strain and thermal expansion, respectively. Since the Bragg wavelength, λ_B is a function of the average refractive index and grating pitch, any change in these variables will cause the Bragg wavelength to shift meaning that the center wavelength of the reflected spectrum changes. Expanding Eq. 2.2 into a Taylor series yields the differential change in the Bragg wavelength resulting from applied strain and temperature variations as in Eq. 2.3.

$$\frac{\Delta\lambda_B}{\lambda_{B0}} = \left(\frac{1}{\Lambda}\frac{\partial\Lambda}{\partial l} + \frac{1}{n}\frac{\partial n}{\partial l}\right)\Delta l + \left(\frac{1}{\Lambda}\frac{\partial\Lambda}{\partial T} + \frac{1}{n}\frac{\partial n}{\partial T}\right)\Delta T \tag{2.3}$$

where Δl is the change in the length of the grating section and λ_{B0} is the reference Bragg wavelength of the unstrained FBG sensor. Here, the terms $(\partial\Lambda/\partial l)$ and $(\partial n/\partial l)$ correspond to a change in the grating spacing due to strain, and the strain-optic induced change in the refractive index, respectively. The terms $(\partial\Lambda/\partial T)$ and $(\partial n/\partial T)$ represent the change in the grating spacing due to the thermal expansion and the thermo-optic induced change in the refractive index, in the given order. Defining thermal expansion and thermo-optic coefficients for an optical fiber as $\alpha_\Lambda = (1/\Lambda)(\partial\Lambda/\partial T)$ and $\alpha_n = (1/n)(\partial n/\partial T)$, respectively, we may write the shift in Bragg wavelength due to a temperature change as in Eq. 2.4.

$$\Delta\lambda_B = \lambda_{B0}(\alpha_\Lambda + \alpha_n)\Delta T \tag{2.4}$$

where α_Λ and α_n are the thermal expansion and the thermo-optic constants, respectively. The shift in Bragg wavelength because of strain can be written as Eq. 2.5 [18].

$$\Delta\lambda_B = \lambda_{B0}(1 - p_e)\varepsilon_x \tag{2.5}$$

where ε_x is the axial strain and p_e is the effective photo elastic coefficient defined as Eq. 2.6 [18].

$$p_e = (n^2/2)\{p_{12} - \nu(p_{11} + p_{12})\} \tag{2.6}$$

where p_{11} and p_{12} are the components of strain-optic tensor, and ν is the Poisson ratio.

If an FBG sensor is embedded into a structure, strain will change the spacing between the gratings which shift the Bragg wavelength. While knowing the Bragg wavelength before the applied strain, the amount of strain applied to the structure can be deduced from the shift in the Bragg wavelength. However in an environment where the structure is exposed to both temperature change and strain, the effects of strain and temperature change on the FBG sensor should be separated. A common way of compensating the temperature effect is to use two FBG sensors that are very close to each other [36, 63]. One of the FBG sensor is encapsulated so that it does not sense the applied strain whereas the other sensor senses both temperature change and sensor. The temperature effect compensation by using two FBGs are detailed in Eqs. 2.7, 2.8 and 2.9.

The Bragg wavelength shift equation can be simplified from Eq. 2.3 as Eq. 2.7.

$$\Delta\lambda_B = (k_{\varepsilon 1})\varepsilon_x + (k_{T1})\Delta T \tag{2.7}$$

where $k_{\varepsilon 1}$ and k_{T1} are strain sensitivity and temperature sensitivity of an FBG sensor, respectively. The equation for an FBG temperature sensor which is fabricated to sense only strain can be written as in Eq. 2.8.

$$\Delta\lambda_B = (k_T)\Delta T \tag{2.8}$$

In the case of a system which consists of an FBG sensor sensitive to both temperature and strain changes and an FBG temperature sensor, the strain signal can be separated from the temperature one through combining Eqs. 2.7 and 2.8 whereby obtaining Eq. 2.9.

$$\varepsilon_x = (\Delta\lambda_1 - \Delta\lambda_2 \frac{k_{T1}}{k_{T2}}) \frac{1}{k_{\varepsilon 1}} \tag{2.9}$$

where $\Delta\lambda_1$, k_{T1} and k_ε are the FBG sensor's change in Bragg wavelength, temperature and strain sensitivity, respectively. $\Delta\lambda_2$ and k_{T2} represents FGB temperature sensor's change in Bragg wavelength and temperature sensitivity, respectively. To be able to use Eq. 2.9, the strain and temperature sensitivities of both FBG sensors should be measured beforehand. What has been described just above is the

simplest approach to separate strain signal from temperature one. The temperature compensation or separation has been an active and fertile research direction in the field of optics. For example, Xu et al. used two superimposed FBG sensors with different strain and temperature sensitivities [71]. James et al. [29] spliced two FBG sensors on two different fibers and used the different strain sensitivities of the sensors to distinguish strain. Some researchers used hybrid sensor which combined FBG with different sensors such as long period grating (LPG) [55]. More recently Lima et al. [39] developed a technique for separating temperature and strain by using an FBG with a linearly tapered diameter. As the FBG is strained, the reflected peak broadens allowing for the determination of strain.

2.3.6 Polarization maintaining fiber optic sensors

FBG sensors written on single mode fiber optic cables cannot measure the amplitude and the direction of a multi-axial strain. If an FBG sensor is written on a polarization maintaining (PM) fiber optic cable, in theory, the FBG sensor should be able to measure transversal strain in addition to the longitudional strain. To be able to measure transversal strain with an FBG sensor, FBG sensors written on a polarization maintaining (PM) sensors are proposed to measure multi-axial strain [66, 35].

Every electromagnetic wave on a fiber optic cable has a different mode that solves a different electromagnetic wave equation. Every solution is called transmission mode of the light and it depends on the optical and geometrical properties of the fiber optics [43]. The above mentioned fiber optic sensors were single mode (lowest bound mode) sensors which transmits the light only in one direction. FBG sensors are designed to reflect this lowest mode [44]. An FBG sensor written on a polarization maintaining fiber reflects a spectrum which has two peaks.

The difference between high-birefringence polarization maintaining fibers and single mode fiber optics is that PM fibers has two perpendicular directions which have different refractive indices [44]. These two directions are called slow and fast axes.

Different types of birefringence polarization maintaining fibers are represented in Figure 2.4. In the case of transversal loading, the refractive indices of the axes changes and the distance between two peaks is altered. The distance between two axes are proportional to the transversal strain [30, 7]. Bragg wavelength shifts in PM fibers that occur due to strain are different for every polarization mode and it is dependent on the direction and magnitude of the applied strain. Hence PM FBG sensors promise future in sensing multi-axial strain [74].

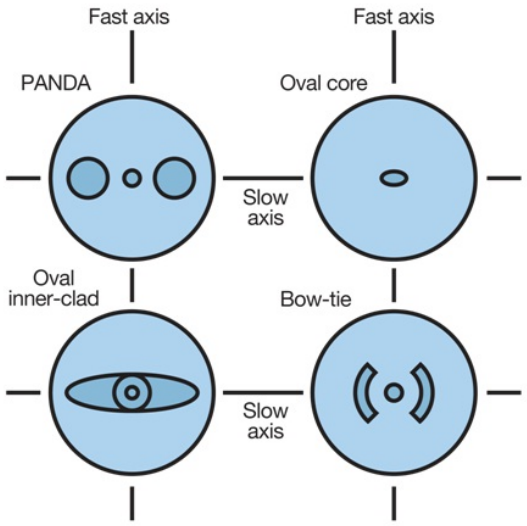

FIGURE 2.4: Different types of PM fibers

The refractive index difference between two axes $(n_s - n_f)$ is called brifringence (B) and it is usually 10^{-4}. Brifringence of a fiber optic is calculated as $(B = B_{IS} + B_E + B_G)$. The B_G is the value of the brifringence due to the fiber's geometry and it is accepted as zero for cylindrical fiber optics. B_{IS} refers to the effect of the internal stress and B_E is the value of the brifringence which is caused by the applied strain on the fiber optic. B_E is calculated by the formula $(B_E = C(\sigma_x + \sigma_y))$. C is the stress-optic coefficient for the fiber optics and σ_x and σ_y are the principle stresses on the fiber. All types of fiber have brifringence value. However it is not desired for single mode fiber optics and it is usually accepted as zero. Two equations of wavelengths of two peaks resulted from an FBG sensor on a PM fiber is written as Eq. 2.10 [44].

$$\lambda_s = 2n_s\Lambda, \lambda_f = 2n_f\Lambda \tag{2.10}$$

From this equation, the difference between two wavelengths can be written as Eq. 2.11.

$$\lambda_s - \lambda_f = 2(n_s - n_f)\Lambda = 2B\Lambda \tag{2.11}$$

In case of any loading, only B_E value increases and this increase results in shift in the difference between two wavelengths [14]. Strain-optic equations are employed to calculate the shift on any of the axes' Bragg wavelength. Strain-optic equations are written as Eqs. 2.12 and 2.13 [44, 65].

$$\Delta\lambda_s = \lambda_{s0}[\varepsilon_z - \frac{n_s^2}{2}(p_{xx}\varepsilon_z + p_{xx}\varepsilon_x + p_{xy}\varepsilon_y)] \tag{2.12}$$

$$\Delta\lambda_f = \lambda_{f0}[\varepsilon_z - \frac{n_s^2}{2}(p_{yz}\varepsilon_z + p_{yx}\varepsilon_x + p_{yy}\varepsilon_y)] \tag{2.13}$$

where ε is the applied strain and p_{ij} are the components of the strain-optic coefficient tensor for an optic fiber. These coefficients are dependent on the materials of the optic fibers. In Figure 2.5, the difference between single mode and PM fiber optics are shown in the case of transversal load.

2.3.7 Application of embedded fiber optics in composite materials

The emergence of fiber optic sensors created different approaches to the structural health monitoring of composites. Although they were first used on the surfaces of materials to be monitored, the ability of embedding fiber optic sensors into composite materials led to the utilization of fiber optic sensor for different purposes. Compared to other methods, fiber optic sensors neither alters the host materials' mechanical properties nor deteriorate the structural integrity or reliability of the structure due to their rather small size.

Structural health monitoring of a composite material starts from the manufacturing phase with flow and cure monitoring. Following the production, the state of the composite material is monitored for the existence and extent of the damage.

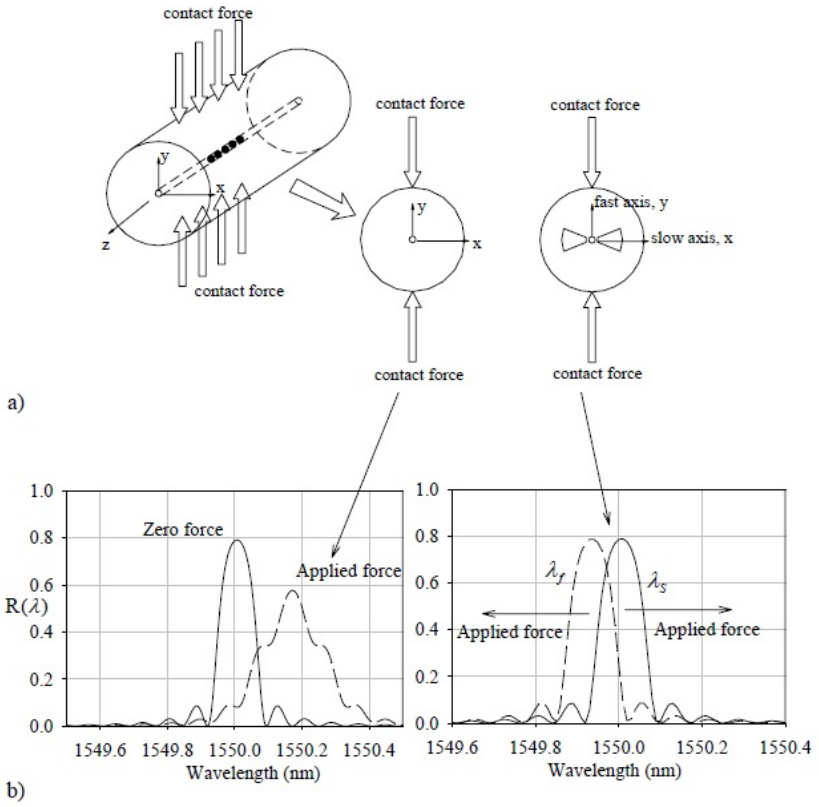

FIGURE 2.5: The behavior of both single mode and PM fibers in the case of transversal load [15]

Usually these three monitoring stage are carried out by different methods and probes. Fiber optic sensors revolutionized structural health monitoring concept by accomplishing the monitoring of these three with a single type of sensor. Another difference made by fiber optic sensors was that they can provide information on a local scale. Before the employment of fiber optic sensors, the state of the composite material was predicted in global scale and other types of sensors and approaches did not give any information about the state of any desired location in a composite materials. The coming subsection provides comparison between traditional monitoring techniques and application of embedded fiber optic sensors. Furthermore, it presents information on the most commonly used fiber optic sensors for structural health monitoring.

2.3.7.1 Flow monitoring

Liquid composite molding (LCM) is a widely used class for manufacturing composite materials. The two well known members of LCM class are resin transfer molding (RTM) and vacuum assisted resin transfer molding (VARTM) methods. In LCM, the layers of fibers are placed inside a mold and then the mold is sealed, for RTM process with a rigid lid and for VARTM with a flexible cover. Subsequently, the resin is injected into the mold. To be able to manufacture an engineeringly reliable composite material without any dry spots, or bubble entrapment, all of the fiber layers should be saturated with resin. Industrial RTM molds are in general manufactured out of non-translucent materials, hence, flow front is visually not accessible. Traditionally, complete mold filling is ensured through operator skill developed over many trial and error runs. This emphasizes the necessity of a method or approach for 100% saturation of fiber reinforcements so that the number of wasted composite parts can be reduced. Fiber optic sensors are suitable candidates for being used to sense resin flow fronts. Optic sensors can be embedded inside the composite material between different layers to be able to monitor the saturation level of the mold thereby reducing the extra usage of resin to saturate the composite.

In literature, over the years, different derivatives of fiber optic sensors have been developed for monitoring the resin flow front as well as mold saturation level. In 1997, Bernstein et al. [4] developed a new fiber optic sensor to sense the resin arrival.They created gaps on a long fiber. In this sensor configuration, light sent travels the fiber by crossing the gap where some light is reflected. When the resin is injected and starts to fill the gaps, more light is transmitted through the fiber. An optical time domain refractometer is used to interrogate the sensor by monitoring the light intensity of the reflected light. Their result proved the ability of this sensor to sense resin arrival.

Antonucci et al. [2] used a Fresnel sensor for flow monitoring. Fresnel sensor is a bare fiber with a cleaved end and reflected light instensity from the cleaved end is dependent on the medium surrounding the sensor. They placed Fresnel sensor

between the layers of fibers in resin film infusion process and monitored the light intensity. The results showed that the resin arrival change the light intensity of the Fresnel sensor.

Long period fibers (LPG) were embedded into the composite to monitor the flow front as well as the curing of the resin. LPG sensors are similar to FBG sensors except the fact of coupling the light out of the core region. The resin alters the amount of light coupled out of the core and results in transmitting more light through the fiber. Dunkers et al. [19] embedded two LPG sensors in an RTM mold and monitored the reflected spectrum with an optical spectrum analyzer. Eum et al. [21] used the same idea as Dunkers. However, they utilized the optical frequency domain instead of measuring the wavelength and the amplitude of the reflected spectrum. Both researches proved the flow monitoring of LPG sensors in composite materials.

Etched fiber sensors (EFS) are one of the common fiber optic sensors that are used in flow monitoring. Their inexpensiveness and relatively easy manufacture process caught some researchers' eye. Ahn et al. [1] used EFS to monitor the flow of the resin in RTM 3D mold in different locations. The mold was made transparent so that the results were verified visually. Keulen et al. [33] and Yildiz et al. [75] modified the EFS sensor by etching some portion of the cladding region instead of etching the whole cladding region in order to decrease the possibility of breakage. Hence the sensors were looped to bend the etched region and make it more sensitive to resin arrival.

FBG sensors were also employed to monitor flow front by utilizing the temperature and strain sensitivity of Bragg wavelength [23]. As the resin reaches the FBG region, it induces a thermal differentials on the FBG. Keulen et al. [33] combined the EFS and FBG sensors on a single fiber to comprehensively monitor the flow front in 2D and 3D RTM mold.

2.3.7.2 Cure monitoring

Once the mold is saturated with the resin, the curing process begins. The curing stage is very crucial in manufacturing composite materials as they took relatively longer time. In the case of a production line of composite materials, the curing time should be calculated so that the composite is not taken out of the mold before the curing process is completed. On the other hand, sometimes composite is kept in the curing process more than necessary which decreases the number of manufactured composite materials. Curing process of resin is an exothermic reaction and temperature keeps increasing as the curing continues. The rise in the temperature stops and starts to decrease as the curing is finished. In most of the cases, this stage marks the ending of the production. Therefore if the temperature is monitored, one may optimize the manufacture of a composite material.

Roberts [56] presented conventional methods to directly monitor curing process. These methods include thermal and dynamic analysis. Additionally, some chemical compounds are added to the resin system and the changes of color, absorbance and transmittance dependent upon time and temperature during cure is monitored. Electrical measurements and dielectric analysis also proved to be another way to monitor curing. The major problem with these methods is that they provide information on a global scale as it was with the flow monitoring. Furthermore adding chemical compounds to the resin change the integrity of the composite and affecting its properties.

In addition to their ability of flow monitoring, embedded fiber optics offer new possibilities to the cure monitoring. A wide variety of fiber optic sensor based methodologies have been investigated for monitoring the cure cycle of resins such as those based on Raman spectroscopy, acuostic wave technique, ultrasonic wave technique, evanescent wave spectroscopy, fluorescence spectroscopy, extrinsic Fabry-Perot interferometer, Fresnel based refractometry and fiber Bragg gratings [65].

Raman spectroscopy is one of the suggested methods used by various researchers [46, 41, 42]. However the results were not satisfactory concurrently the insertion

of fiber optics were too hard and hostile to the material. Acoustic wave based technique is another method that was employed to cure monitoring. The idea is to generate ultrasonic waves on the composite which will travel through the material and sensed by a fiber optic sensor. The properties of the wave changes as the resin cures hence enabling the monitoring the process. Additionally, Davis et al. [11] used a fiber optic cable to heat the composite by a laser which resulted in ultrasonic waves. The speed of the waves were monitored by a Michelson interferometer. Other types of fiber optic sensors used to cure monitoring was fluorescence monitoring sensors [58, 6, 10, 54], sensors based on an evanescent wave [8, 70, 48], extrinsic Fabry-Perot interferometer (EFPI) sensor [22], Fresnel sensor [9] and LPG sensor [19].

Fiber Bragg gratings have been used extensively by various researchers for cure monitoring by [16, 45, 31, 20] among others. This is partly due to the fact that if implemented appropriately FBGs can be used for flow monitoring, cure monitoring and structural health monitoring [33]. Most techniques focus on the structural health monitoring considering the process monitoring a secondary bonus.

Dunphy et al. [20] were among the first to investigate FBGs for cure and strain monitoring of composites in 1990. Murukeshan et al. [45] also investigated the potential of FBGs for cure monitoring. Their technique was to simply place the FBG sensor inside the laminate and monitor the shift in Bragg wavelength during the curing process. No attempt was made to separate the effects of strain and temperature change, simply to monitor the overall effect on the FBG. Their results show that repeatable curves can be observed and suggest that a deviation from these curves indicate an anomaly in the cure process. Cure monitoring experiments of our group successfully embedded the FBG sensors into the resin transfer molded composite materials for cure monitoring [75]. Several experiments were conducted with placing the FBG sensor between different laminates. Since the cure process is exothermic, the released heat shifts the Bragg wavelength. As the strength of the exothermic process diminishes, temperature of the RTM mold decreases to the preset cure temperature. Given the presence of residual stress buildup in the composite (due to various effects such as thermal gradients, shrinkage, and

differentials in thermal expansion coefficients), the Bragg wavelength does not return to its original value. Eventually the Bragg wavelength slowly decreases until it reaches a steady state which marks the end of the curing process.

2.3.7.3 Damage detection

Damage detection of composite material refers to the part of the structural health monitoring during the service of the composite materials. Embedded fiber optics in the manufacturing process provide continuous information on the situation of the material. In the context of the structural health monitoring, damage refers to the crack propagation, temperature and fatigue induced damage, delamination and impact damage [34].

Crack propagation and delamination of composite materials were monitored by tracking the FBG reflected spectrum [51, 62]. As the crack density grows, reflected spectrum broadens which increases the full width half maximum (FHWM). The theoretical calculations of FHWM was also made to verify that the broadening effect was due to the transversal cracks. Okabe et al. [49] developed a small diameter FBG sensor to detect microscopic damages by inspecting the change in the FHWM of the reflected spectrum. In addition to monitoring the crack growth, Okabe et al. [50] employed chirped FBG sensors to locate the crack growth. Compared to simple FBG sensor, the chirped FBG has different Bragg wavelength values for different locations on the sensor. As the crack grows on the chirped FBG, affected wavelength on the reflected spectrum corresponds to the location of the crack.

Damage detection of fatigue induced damage is explained in the next section. The applications of embedded fiber optic sensors proved to be useful in monitoring the health of the composite structure. Amongst the fiber optic sensors, the FBG sensor appears to be the most applicable and easiest sensor to monitor the whole life of a composite structure.

2.4 Remaining useful life prediction

Data obtained from embedded FBG sensors during the life of a structure can be used to determine the remaining useful life of a composite material. In order to achieve that, an appropriate fatigue life prediction model that is compatible with the data obtained from FBGs should be selected and this model should be implemented to accurately predict the remaining useful life. It appears that Doyle et al were among the first to monitor the reduction in stiffness of composites during fatigue with an FBG [17]. To our knowledge, no work has been done that incorporates embedded fiber optic sensors for remaining useful life prediction on a cycle by cycle basis.

Fatigue of composites has been an area of interest for over forty years. The fatigue behavior of composites is a complex phenomenon due to various types of damage that can occur (fiber fracture, matrix cracking, fiber buckling, fiber-matrix interface failure, delamination, etc.) and interact with each other [24]. Research has shown that the damage process in fiber reinforced composites under fatigue loading is progressive and is a combination of various damage modes. The field of fatigue life modeling of composite materials is extensive, however there is still no widely accepted model that most engineers agree upon. Many excellent references that cover a variety of available models exist such as [24, 64, 12] among others.

As observed by various researchers, the effect of fatigue on the stiffness of fiber reinforced polymer matrix composites follows a trend. This trend can be characterized by three stages as shown in the plot of our test results in Figure 2.6. Stage I is characterized by a sharp, non-linear decrease in stiffness. This is attributed to a rapid interconnection of matrix cracking initiated by shrinkage stresses, degree of resin cure, voids and fiber discontinuities. This stage is generally limited to the first 15-25% of fatigue life. Stage II is characterized by a gradual, linear decrease in stiffness that occurs between 15-20% to 90% of the fatigue life. This decrease is attributed to matrix cracking leading to crack propagation, fiber debonding and delamination. The final stage shows a sharp non-linear decrease eventually resulting in a sudden fiber failure [47, 32]. Interestingly, the very initial stages of fatigue

testing results in an increase in stiffness that is generally attributed to viscoelastic deformation of the matrix allowing for fiber alignment along the axis of loading [59].

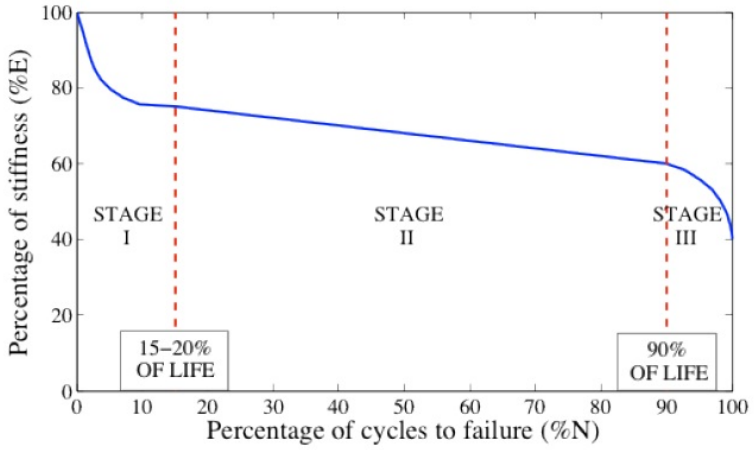

FIGURE 2.6: Stiffness degradation vs. fatigue cycle

Researchers have shown that $S-N$ curves of unidirectional composites have virtually no clear threshold stress level as established in metals, however it is recognized that a certain threshold level of strain in resin does exist for indefinite fatigue life although it is very low, around 5-10% of the ultimate strain [47]. Hence, life prediction models based on $S-N$ curves may not be applicable for fiber reinforced plastic (FRP) composite materials.

A small number of models will be described here in an attempt to demonstrate why the strain energy release rate model was selected as well as to give an idea of the variables involved in such models and how they are applied. This is by no means a comprehensive coverage of the subject.

One of the first fatigue life models was proposed by Hashin and Rotem [57] as: $\sigma_A = \sigma_A^u$ and $\left(\frac{\sigma_T}{\sigma_T^u}\right)^2 + \left(\frac{\tau}{\tau^u}\right)^2 = 1$, where σ_A and σ_T are the stresses along the fibers and transverse to the fibers, τ is the shear stress and σ_A^u, σ_T^u and τ^u are the ultimate tensile, transverse tensile and shear stress, respectively. Because the ultimate strengths are functions of the fatigue stress level, stress ratio and number of cycles the criterion is expressed in terms of three $S-N$ curves that

are determined experimentally. The criteria are only valid for laminates with unidirectional plies.

Much research was done on phenomenological models to predict the stiffness degradation of composites by Whitworth [67, 68], and Yang [72]. Hwang and Han introduced the fatigue modulus concept [27]. The fatigue modulus concept is described as the slope of applied stress and resultant strain at a specific cycle. The degradation rate of the modulus is assumed to follow a power function: $\frac{dF}{dn} = -Acn^{c-1}$, where F is the fatigue modulus, n is the number of cycles and A and c are material constants. They assume that the applied stress σ_a varies linearly with the resultant strain such that: $\sigma_a = F(n_i)\varepsilon(n_i)$, where $F(n_i)$ and $\varepsilon(n_i)$ are the fatigue modulus and strain at loading cycle n_i, respectively. The strain life, N can be calculated by integrating from $n_1 = 0$ to $n_2 = N$ and introducing the strain failure criteria, which states that failure occurs when the fatigue strain reaches the ultimate static strain to obtain: $N = [B(1-r)]^{1/c}$, where $B = F_0/A$, F_0 is the fatigue modulus at the 0^{th} cycle, A is area, $r = \sigma_a/\sigma_u$ is the ratio of applied cyclic stress to ultimate static stress and c is a material constant. Hwang and Han also proposed three cumulative damage models based on the fatigue modulus [28]. Lee used a stiffness degradation model to predict failure [37].

Whitworth used the residual stiffness model to propose a cumulative damage model [69]. In this model the damage function is defined as: $D = \left[\frac{H\cdot(1-\overline{S})^a}{1-\overline{S}^a}\right] \cdot \frac{n}{N}$, where $\overline{S} = S/R(0)$ is the normalized applied stress range, $R(0)$ is the ultimate strength, S is the applied stress range and a and H are parameters. When $D = 0$ no cycles have been applied and when $D = 1$ failure has occurred. This model degenerates into the Miner damage model when a becomes unity, i.e. when the stiffness degrades linearly until failure. This model has been extended to predict the remaining life of specimens subject to variable amplitude loading. Whitworth used the variable amplitude approach to convert a number of cycles at a particular stress to a number of cycles at a reference stress. These stress values are summed and when the values equal one, failure occurs [69].

The aforementioned models take factors such as stress, strain, stiffness and number of cycles and develop abstract material properties to develop a formulation. Other researchers have investigated other properties as an indication of fatigue. The challenge with these models is that they all require knowledge of the load/stress applied to the composite. With FBG sensors this data is not available; only the strain is sensed.

2.4.1 Application of fatigue life prediction models to FBG based RUL

The relevant data collected from an FBG is in the form of strain and number of cycles. As described above, the stiffness of composite materials under fatigue loading gradually decreases over time. This means that the modulus of elasticity is not constant, it is a function of the load history and the stress-strain relationship (Hooke's law) can no longer be applied to extract the magnitude of stress from strain. Therefore a suitable model cannot use stress as an input; it must use the strain.

A promising method of predicting the remaining useful life using only strain was developed by Natarajan et al [47]. The method relies on the strain energy release rate and takes advantage of the fact that it is linear throughout Stage II. It follows a similar approach to the fatigue modulus concept proposed by Hwang and Han [27].

To apply this model the material must be characterized to obtain a relationship between applied strain, ultimate strain and the energy release rate. The method assumes that there is a specific amount of strain energy in the material that is released before it enters Stage III, at which point it is past its useful life. The strain energy can be determined before fatigue loading and used to predict the number of cycles to failure. An example of the progression of the release of strain energy from a composite during fatigue is shown in Figure 2.7. This method can be employed as a cumulative model if the energy is summed over each cycle. In

this research it is proposed to use this method to calculate the released energy on a per-cycle basis using strain data obtained from embedded FBGs to predict the remaining life. The complete derivation of this method is presented in [47]. An abbreviated version is presented here along with a modification so it can be applied to FBG acquired strain/cycle data.

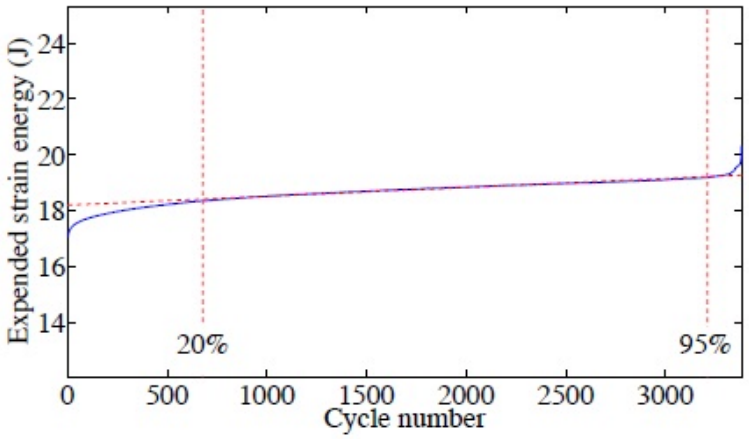

FIGURE 2.7: Expended strain energy during fatigue loading

The variation of expended energy can be described as:

$$\frac{dU_j}{dN_j} = f(\varepsilon_m, \varepsilon_{sr}, U_j, C_t) \tag{2.14}$$

where U_j is the expended energy, N_j is the load cycle, ε_m is the mean strain, ε_{sr} is the strain range, C_t is the composite type. Eq. 2.14 can be written in terms of the number of cycles:

$$N_j = \int_{U_0}^{U_j} \frac{dU}{f(\varepsilon_m, \varepsilon_{sr}, (U_j - U_0, C_t))} \tag{2.15}$$

where U_0 is the initial strain energy prior to fatigue initiation and:

$$U_j = U_0 \cdot g(\varepsilon_m, \varepsilon_{sr}, (U_j - U_0), C_t) \tag{2.16}$$

where the function: $g(\varepsilon_m, \varepsilon_{sr}, (U_j - U_0), C_t)$ must be determined experimentally. Differentiating Eq. 2.16 with respect to N_j:

$$\frac{1}{U_0}\frac{dU_j}{dN_j} = g'\left\{\varepsilon_m, \varepsilon_{sr}, (U_j - U_0), C_t\right\} \cdot f\left\{\varepsilon_m, \varepsilon_{sr}, (U_j - U_0), C_t\right\} \tag{2.17}$$

and rearranging Eq. 2.17:

$$f\left\{\varepsilon_m, \varepsilon_{sr}, (U_j - U_0), C_t\right\} = \frac{1}{U_0}\left(\frac{dU_j}{dN_j}\right)\left(\frac{1}{g'\left\{\varepsilon_m, \varepsilon_{sr}, (U_j - U_0), C_t\right\}}\right) \tag{2.18}$$

The right hand side of Eq. 2.18 must be evaluated for ε_m, ε_{sr} keeping the other parameters constant.

The energy release rate: dU_j/dN_j (the rate of energy expended per load cycle) is linear throughout Stage II, therefore the energy release rate for the material at various strain levels can be determined experimentally. The function: $f(\varepsilon_m, \varepsilon_{sr}, U_j, C_t)$ can then be determined by plotting the variation of the energy release rates with maximum induced strain.

The data obtained during fatigue loading should be load and deflection. This data is then used to calculate the strain energy U_n at any cycle: $U_n = \frac{P_n \delta_n}{2}$, where P_n is the load at n cycle and δ_n is the deflection at n cycle.

The amount of energy released at 90% of the life cycle (when the material enters Stage III) compared to the initial amount of energy changes based on the ratio: $r = U_f/U_0$. Failure is assumed to occur at this point as the material is no longer intact and dangerously close to catastrophic failure, therefore: $N_f = N_{90\%} = 0.9N_{ult}$.

The slope of Stage II is the expended energy per cycle or the energy release rate: dU/dN. This can be obtained for each specimen by performing a regression analysis of the expended energy data in Stage II. The energy release rate is found to be constant and is characteristic of the constitutive material under similar loading conditions and increases with an increase in induced strain.

Experimental data of the variation in energy release rates with normalized maximum induced strain is fit to a power law:

$$\frac{dU}{dN} = a\left(\frac{\varepsilon_{max}}{\varepsilon_{ult}}\right)^b \tag{2.19}$$

where ε_{max} is the maximum induced strain of the material, ε_{ult} is the ultimate static strain of the material (assumed to remain constant throughout the lifetime) and a and b are fatigue coefficients.

Since the coefficients a and b are invariant for a particular material under a given load type, the fatigue life can be written as:

$$N_f = \frac{U_0 - U_f}{a(\varepsilon_{max}/\varepsilon_{ult})^b} \tag{2.20}$$

where U_0 is the initial strain energy of the material at ε_{max} before fatigue loading, U_f is the sum of the expended strain energy at the end of Stage II and N_f is the fatigue life just before entering Stage III.

Since the specimen is loaded linearly up to the mean strain level before applying fatigue load, the expended energy of the material before fatigue loading is the energy at the mean level. The energy of the material at 0 cycles can be written as:

$$U_0 = \frac{P_{mean}^2 l}{2AE} \tag{2.21}$$

where P_{mean} is the mean level of the cyclic load, E is the modulus of elasticity in the loading direction, l is the span (gage length) and A is the cross sectional area. The fatigue life of a material can be obtained experimentally for a particular loading from Eqs. 2.15 and 2.19, at N_f and written as:

$$N_f = \frac{U_0 - rU_0}{a(\varepsilon_{max}/\varepsilon_{ult})^b} = \frac{(1-r)U_0}{a(\varepsilon_{max}/\varepsilon_{ult})^b} \tag{2.22}$$

Life prediction can be accomplished by summing the energy released under various load amplitudes for the corresponding number of cycles and finding N_f after inserting the total expended energy into Eq. 2.22. In the case of an FBG based SHM

system, the magnitude of the strain is sensed on every cycle. With this method it is possible to sum the energy on a cycle-by-cycle basis using data obtained from the FBG.

To calculate the energy released during one cycle, Eq. 2.19 is integrated with respect to N over one cycle, ie. from N_j to N_{j+1} and ε_{max} is replaced with $\varepsilon_j^{(FBG)}$, the maximum strain value recorded by the FBG during cycle j. This leads to:

$$\Delta U_j = a \left(\frac{\varepsilon_j^{(FBG)}}{\varepsilon_{ult}} \right)^b \tag{2.23}$$

when $(N_{j+1} - N_j) = 1$.

The energy released during each cycle can then be summed during the life of the composite to get the total expended energy up to that cycle: $U_{expended} = \sum_{j=1}^{n} \Delta U_j$. The remaining life can be estimated: $U_{remaining} = (1-r)U_0 - U_{expended}$, where $U_{remaining}$ is the remaining energy left in the material before failure. Eq. 2.20 can be modified to convert the remaining energy into the number of remaining cycles:

$$N_{n-f} = \frac{U_{remaining}}{a(\varepsilon_{expected}/\varepsilon_{ult})^b} \tag{2.24}$$

where N_{n-f} is the remaining life at cycle n, $\varepsilon_{expected}$ is the expected strain level for the remainder of the life. For example, $\varepsilon_{expected}$ could be the average maximum strain from the previous portion of life or if the component was expected to be under harsher loading, $\varepsilon_{expected}$ would be greater than the average maximum strain. With Eq. 2.24 various fatigue cycle scenarios could be predicted for various loading cycles by modifying the value of $\varepsilon_{expected}$. The addition of Eqs. 2.23 and 2.24 to the fatigue life prediction technique developed by Natarajan [47] allow for a stepwise addition of expended energy. This is a novel approach to remaining useful life prediction that allows a prediction to be made at each cycle.

Chapter 3

Embedded Optical Fiber in Composite Materials

3.1 Introduction

In this chapter, we have explained the resin transfer molding method which is employed for producing composite materials for the present work. Additionally, the method of embedding optical fibers into the composite materials and health monitoring of the composite structures are presented.

In the first section of this chapter, the resin transfer molding system in our lab is presented with different configurations; namely, for 3 mm thick composite panels, 2 mm thick carbon fiber reinforced composite panels and hollow square and semi-circle beams. Thereafter, the procedure for the fabrication of composite specimen is described. In the second section, the ingress-egress technique for embedding fiber optics in composite materials, process monitoring of composite manufacturing step and health monitoring of the composite structures are demonstrated. Although it has not been embedded into the composite materials, we also presented the results of the experiments with PM FBG in this section.

3.2 Resin transfer molding

The RTM method can produce complex, high quality, near net-shape parts in series production with high fiber volume fractions, a class A surface finish and little post processing. In this process, a fiber preform (glass or carbon) is placed in a closed mold and resin is injected into the mold to saturate the preform. After the resin cures, the mold is opened and the final composite part is de-molded. A pressure pot is used to inject the resin, the RTM mold is heated via a water heater and a vacuum pump is used to remove air from the system. Our RTM apparatus has a glass viewing window which enables us to see the flow of the resin. Manufacturing composite materials in different sizes and shapes are possible via changing the mold. In this thesis work, we have manufactured 2D composite panels with different thicknesses and 3D hollow square beams. Figure 3.1 and Figure 3.2 shows a schematic of the RTM process together with the lab scale in-house built RTM system.

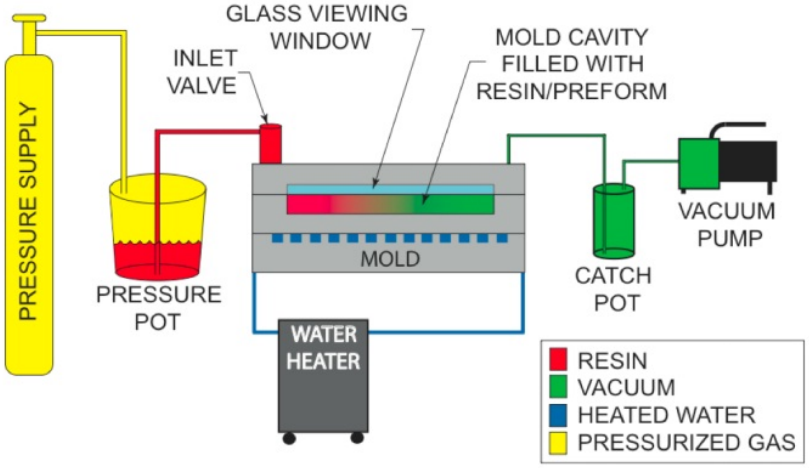

FIGURE 3.1: Schematic of RTM system

3.2.1 Experimental apparatus of 2D

Composite panels are manufactured with 2D mold which produces a 305mm x 610mm x 3.5mm specimens. Specimens manufactured with these dimensions are glass fiber reinforced composites (GFRC). These specimens were used in damage

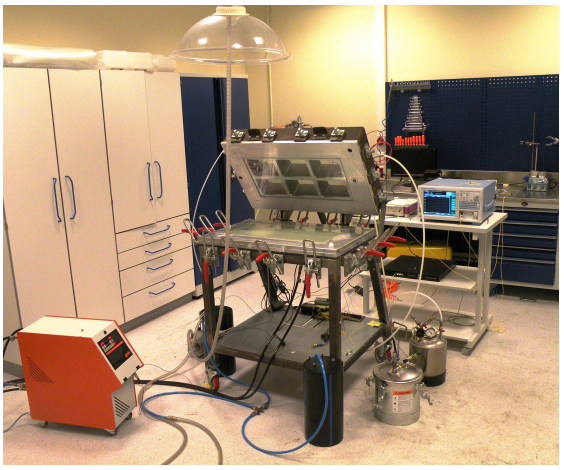

FIGURE 3.2: Inhouse built RTM system

detection and fatigue monitoring studies within the scope of this thesis work. The results of these experiments are explained in detail in chapter 4 and 5. An example of GFRC panel inside the mold is shown in Figure 3.3. The details of the manufacturing of the RTM system and composite panels are presented in another thesis from our laboratory [53].

FIGURE 3.3: Manufactured 2D GFRC panel

2-D composite plates with carbon fiber reinforcements are also manufactured for the purpose of conducting fatigue experiments to study the remaining useful life model presented in the previous chapter. To be able to stay within the loading capacity of the fatigue machine, carbon fiber reinforced composite (CFRC) plates are manufactured with 1.7mm thickness since the CFRCs are much more rigid and stronger in comparison to glass fiber reinforced composites for the same volume fraction of the reinforcement. Hence, the RTM mold has been modified by placing

an Al plate to mold cavity to reduce the depth of the mold cavity. Figure 3.4 shows carbon fibers are placed inside the thinner mold before injection.

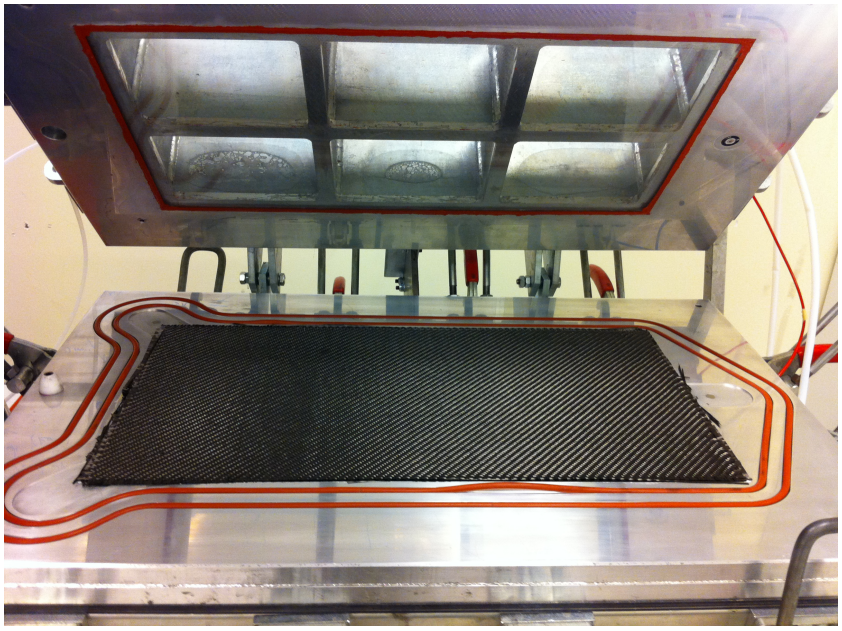

FIGURE 3.4: A 2D CFRC before injection

3.2.2 Experimental apparatus of 3D

Composite materials used in the industry are usually in complex shape. Therefore, in this work, we would like to prove that the ingress/egress method used for inserting the FBG sensors into 2-D composite plates can be readily applied 3D composite materials. In this regard, a 3D mold is designed and manufactured such that a hollow square beam with dimensions of 510mm x 35mm x 2.5 mm and a hollow semicircle beam with 510mm x 17.5mm x 2.5mm would be produced simultaneously or individually. In Figure 3.5 integrated 3D mold into the RTM system as well as square and semi-circle mandrels required for creating hollow geometry are presented.

To be able to use the 3-D mold in the RTM system originally designed for 2-D mold, hinges that connect the mold and the lid are redesigned and manufactured since the 3D mold is thicker than the 2D mold. New hinges that were used in 3D mold is shown in Figure 3.6.

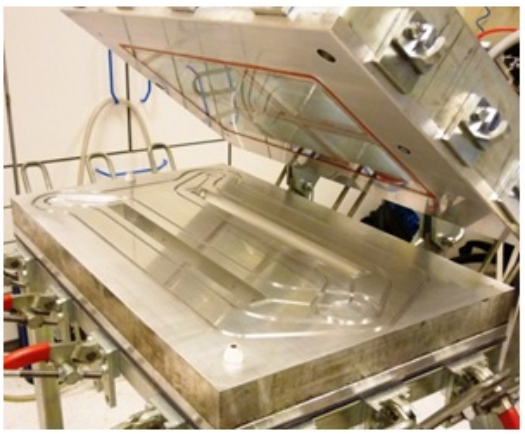

FIGURE 3.5: *a)* 3D mold inside the RTM system, *b)* Square and semicircle mandrels

FIGURE 3.6: Hinge that connects the lid and the mold

Semicircle and square mandrels are manufactured in 3-axis CNC at Sabanci University Machine Shop after the design phase. Materials of the mold and mandrel are the aluminum alloy known as AL 6061. This material is chosen due to its higher resistance to scratches compared to standard industrial aluminum alloys. After the manufacturing process, the surface of the mold and mandrels are sandpapered by increasing the mesh size of the sandpaper to achieve high surface quality. Following the surface cleaning with AXEL/XTEND SX-500 cleaner, AXEL/XTEND S-19C sealer was applied several times to all surfaces carefully to fill micro holes on surfaces. Before each production of composites, AXEL/XTEND 818 release was applied to the surface several times to ensure that the cured resin will not

stick to the mold and the part would be easily demolded.

3.2.3 Specimen fabrication

The specimen fabrication consists of five stages; namely, preparation of the fabric, injection, curing, post-curing and demolding the final product. Additionally, 3D composite specimens need an extra stage where the mandrel is removed. Except for the preparation of the fabric and demolding the final product, the process is the same for both 2D and 3D specimens.

The manufacturing of a 2D composite specimen is easier than a 3D composite specimen. For 2D specimen, fiber reinforcement is cut to the rectangular size of the mold cavity through using a circular razor blade with the help of a rectangular shaped aluminum template. In composite manufacturing, the cutting process should be done tediously so that the edges of the cut layers should not be damaged. Otherwise, once the fiber layers are placed into mold, the cut edges will not meet nicely with side surfaces of the mold thereby leaving openings or gaps thereof. This situation will lead to race tracking in these regions during the injection process, hence resulting in non uniform flow front, and in turn dry-spots in the manufactured composite panels. During placing the fiber reinforcement layers into the mold cavity, fiber optic sensors can be embedded between the layers of interest. As for the manufacturing of the 3-D composite structure, two sets of fabric is cut in dimensions of 800mm x 600m x 650mm x 500mm. Wrapping the mandrel carefully with the fabric around is crucial. In Figure 3.7, the wrapping procedure for square mandrel is presented. The fabric is wrapped around the mandrel for twelve times to produce a composite beam with 2-2.5 mm wall thicknesses. Each fabric layer is approximately 0.2 mm. The wrapped fiber layers are kept in place by applying residual amount of adhesive to the end of the final layer. Before inserting madrel wrapped by the fabric into the mold cavity, two layers of fabric are placed into mold cavity, and subsequently FBG sensors are positioned on these layer at appropriate positions. The details of the ingres/egress methods for FBG sensors

are given in the coming section. Finally,the lid of the RTM system is closed and resin injection process is initiated.

FIGURE 3.7: Wrapping the fabric around the square mandrel

Throughout this work, the resin system composed of LY564 epoxy resin and XB3403 hardener from Huntsman Advanced Composites is employed. The weight ratio of the resin and hardener is 100 to 36 which means that for every 100 gr usage of epoxy resin, 36 gr of hardener is used. The epoxy resin and hardener are weighed on a sensitive scale and mixed inside a polyethylene liner to be placed into the pressure pot. Before starting the injection process, it is ensured that the RTM system is airtight, and the resin system in the pressure pot as well as the mold cavity are degassed by a vacuum pump. Resin injection continues until the mold is fully impregnated which can be concluded through glass window and until the resin comes out of the venting ports without any bubble in it. Having ensured that no entrapped air bubbles are available within the composite panel, the injection process is terminated and outlet ports are closed. Subsequently, curing cycle is initiated by heating the mold to 50° Celsius via water heater. After 12 hours

of initial curing at 50° Celsius, the mold temperature is raised to 80° Celsius and kept at this temperature for 12 hours. As can be concluded, it takes roughly two or three days to manufacture a composite specimen.

The demolding of the 2D composite specimens is relatively less problematic in comparison to that of 3-D final products. In any case, the demolding process should be performed carefully so that FBG sensors should not be damaged. Since the 3-D product is inserted into a deep mold cavity, it is impossible to remove it off the mold cavity from its top surface. In the RTM system, there are several holes through which pressure sensors are mounted to the mold from the bottom. After the lid of the RTM system is opened, the pressure sensor fittings are dismounted from the mold, and this holes are used to insert push pins until the push pins rest on the bottom surface of the composite beam. The push pins are pushed by a hydraulic jack until the composite part pops out of the mold cavity. A metal push pin and a hydraulic jack are shown in Figure 3.8.

FIGURE 3.8: Hydraulic jack and cylindrical metal piece used for removal of the 3D specimen from the mold

After the composite beam with a mandrel is demolded, the mandrel needs to be removed off from the composite beam. Therefore, the system shown in Figure 3.9 is designed and manufactured. Three circular beams in calculated length pushes the mandrel out of the specimen by hydraulic press. Over and under the system, there are square plates that ensures force is perpendicular to the mandrel. The

usage of hydraulic press to remove the mandrel is presented in Figure 3.10. A 3-D square composite specimen with fiber optic sensor is shown in Figure 3.11.

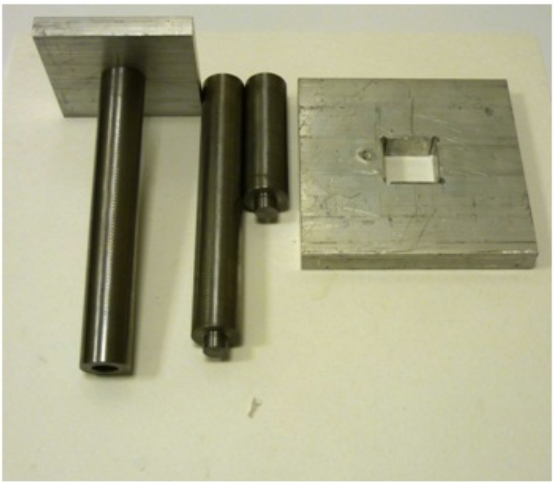

FIGURE 3.9: The system used for removal of the mandrel from the specimen

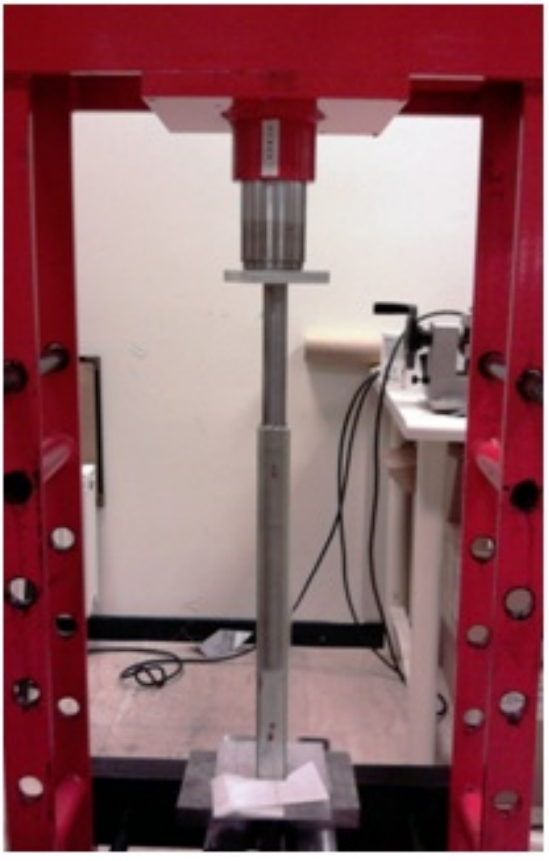

FIGURE 3.10: The process of removal of the mandrel with hydraulic press

In this thesis work, five different 3-D specimens were manufactured. First specimen was produced without any optical fiber, second specimen was manufactured

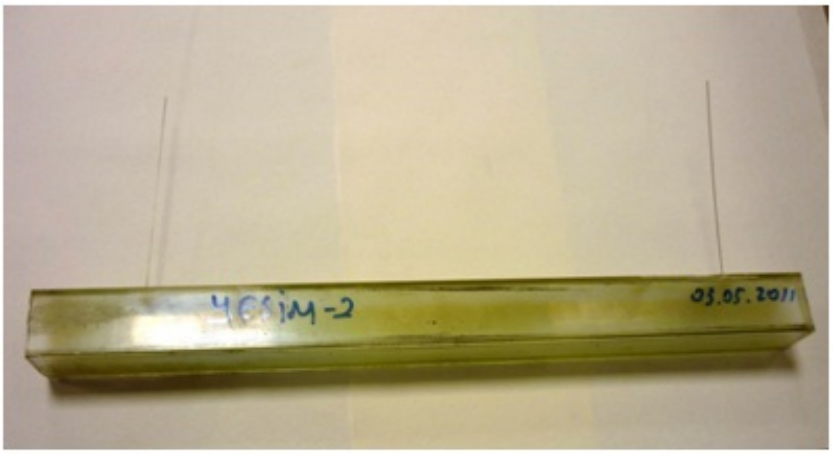

FIGURE 3.11: A 3D composite specimen with fiber optic sensors

with optical fiber without any sensor on it. The other remaining specimens were manufactured with optical fibers with two FBG sensors on them. This attempts have shown that the developed RTM system can produce realistic 3-D composite beam integrated with FBG sensors in repeatable and reliable manner. The characterization and verification of embedded FBG sensors in the 3D specimens will presented in the next section.

3.3 Embedded optical fiber

3.3.1 Ingress/Egress technique

The ingress/egress of fiber optics is one of the important issues for embedding fiber optic sensors into composite structures in a repeatable and consistent manner because the optical fiber is fragile at the ingress/egress location, and does not tolerate a sharp bending radius. Therefore a novel technique developed in our lab to embed the optical fiber sensors in to the composite structure [33, 75]. Due to the closed nature of the RTM method handling the fiber optic sensors are challenging. As the optical fiber sensor enters the mold from below, it sees a 90° radius in order to be parallel to and linear to fabric layers. Optical fibers cannot tolerate this radius, hence we insert the optical fiber inside a thin hypodermic tube in which optical fiber sees less than 90° radius. Furthermore hypodermic tube protects the

optical fiber after the removal of the composite material from the mold. A tapered silicone stopper was used to seal around the hypodermic tube. A custom fitting is used to keep the stopper and fiber in place. In Figure 3.12, the ingress/egress technique is shown.

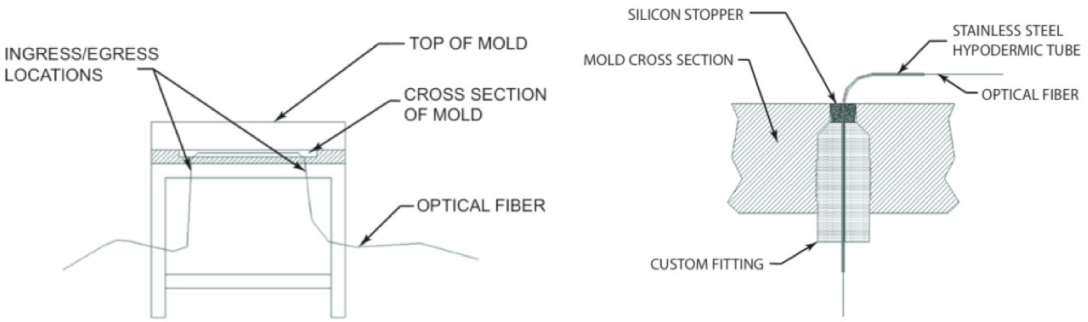

FIGURE 3.12: Path of fiber for through thickness ingress/egress (left), and the schematic of fiber sealing (right)

The technique is similar in both 2D and 3D specimens. Hypodermic tubes are inserted from below after desired layers are placed in the mold and the tubes are given a radius so that it is parallel to the layers. Then the remaining layers are placed on top of the optical fiber in 2D specimen and for 3D specimen mandrel wrapped with remaining fabric is placed. Afterwards, the lid of the RTM system is closed and clamped. In the meantime, the signal from the optical fiber sensor is monitored in order to ensure the integrity of the sensor inside the composite material.

3.3.2 Process monitoring of composite manufacture

Process monitoring of composite manufacturing consists of cure and flow monitoring of the resin inside the RTM system. Although the flow monitoring of 2D RTM mold was the subject of another thesis written in our lab [53], I have contributed to the experiments and we have published our results in a conference [3] and a journal paper [75]. An example of process monitoring of 2D composite manufacture is represented in Figure 3.13. Composite panel had nine layers of biaxial glass fiber reinforcement. FBG sensor was positioned between the fourth and fifth ply. The resin was injected into the mold heated to 50° Celsius. A drop in the

wavelength is observed upon the arrival of the resin to the FBG sensor. As the resin gradually reaches the cure temperature, the Bragg wavelength of the FBG sensors increases. The horizontal line in Figure 3.13 indicates the preset mold temperature. Regardless of experimental conditions, the tendency of wavelength versus processing time is identical, implying the effectiveness of FBG sensors for cure monitoring for RTM composites.

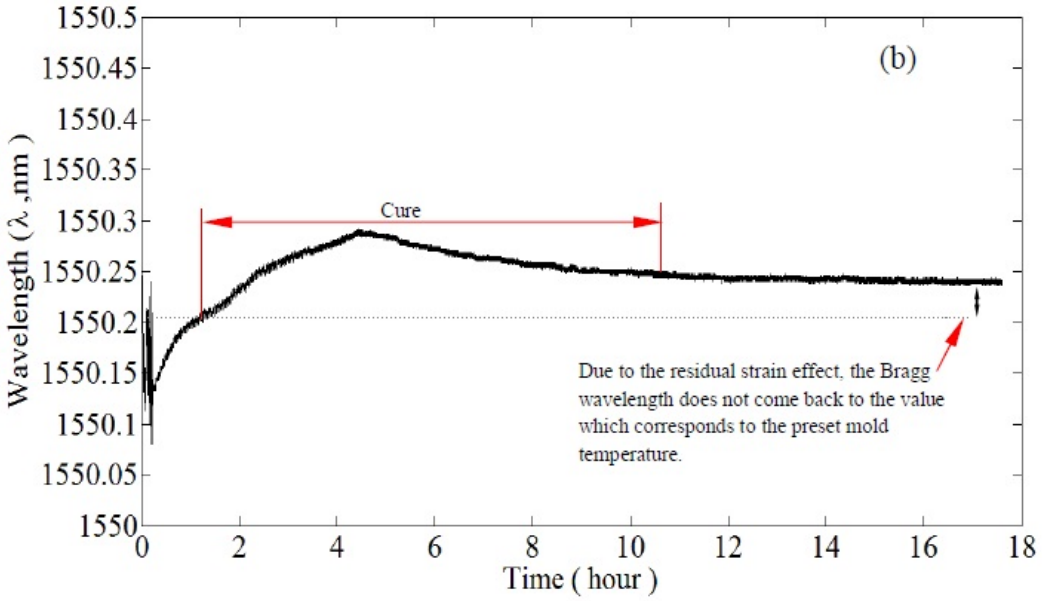

FIGURE 3.13: Process monitoring of 2D composite manufacture by a FBG sensor

3.3.3 Health monitoring of composite structures

As the process monitoring capability of FBG sensors were tested, the health of the composite structures with embedded FGB sensors were tested using tensile and cyclic loading experiments. This stage was very crucial in this thesis because if the embedded sensors were not able to sense the strain in the composite material, damage detection and fatigue monitoring experiments would be impossible. Hence, the study with the embedded sensors was carried out with different composite specimens with different properties.

The 2-D specimens with embedded FBG sensors were used for tensile testing at Sabanci University. The tensile tests were carried out with Zwick/Roell brand

Z100 tensile machine in Figure 3.14. The embedded FGB sensors were monitored with Micron Optics brand sm230 interrogator with the ENLIGHT program and surface mounted Vishay brand 350Ω strain gages were monitored via National Instrument brand NI SCXI-1600 DAQ and NI SCXI-1520 module with LabVIEW SignalExpress program.

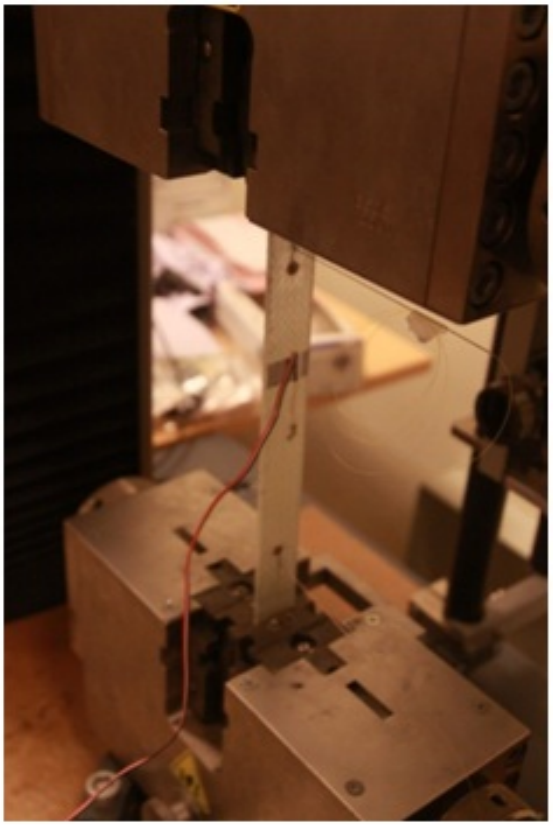

FIGURE 3.14: Tensile test of a 2D specimen in Zwick tensile machine

There are two tensile test specimens which are coded as RTM-10 and RTM-13. In RTM-10 specimen, nine layers of biaxial fabric was used and the embedded FBG sensor with 1550nm as Bragg wavelength was placed between fourth and fifth layers. The dimensions of the specimen was 300mm x 27mm x 3.5mm. The other specimen (i.e., RTM-13) is made of nineteen layers of woven fabric and has an FBG sensor with 1555 nm Bragg wavelength embedded between tenth and eleventh layers. The dimensions of the specimen was 250mm x 25mm x 3.5mm. The specimens are shown in Figure 3.15.

The results of the tensile experiments in the elastic region were processed in MATLAB. The FGB wavelength and strain gage data for RTM-10 were plotted against

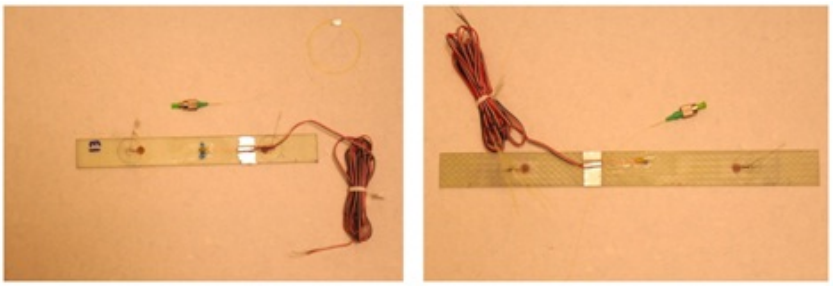

FIGURE 3.15: Tensile test specimens, RTM-13(left) and RTM-10(right)

experimental tensile stress data, respectively, in Figure 3.16 and Figure 3.17. A linear curve was fit to the both data with R^2 value of 0.99. The comparison of Figure 3.16 and 3.17 indicates that the FBG is a linear sensor, which can be further shown by plotting FBG wavelength as a function of corresponding strain gage data as shown in Figure 3.18. Upon using Eq. 2.5, one can determine the photo-elastic constant and strain sensitivity, which are found to be 0.24 and 1.078 nm/mϵ, respectively.

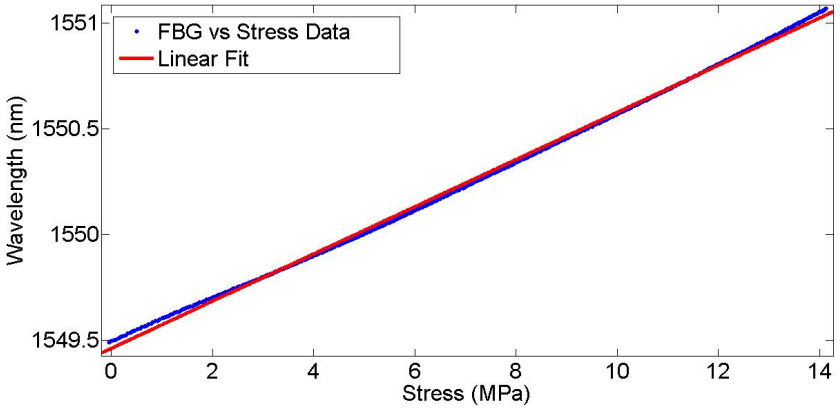

FIGURE 3.16: Wavelength versus stress data for RTM-10

Similar to RTM-10 tensile experiment, the FGB wavelength and strain gage data for RTM-13 were also plotted against stress data from tensile machine, respectively, in Figure 3.19 and Figure 3.20. A linear curve was fit to both data with R^2 value of 0.99. The FBG data was plotted against strain data and a linear curve was fit to the data with R^2 value of 0.99, as shown in Figure 3.21. Again from Eq. 2.5, the photo-elastic constant and strain sensitivity are determined to be 0.24 and 1 nm/mϵ.

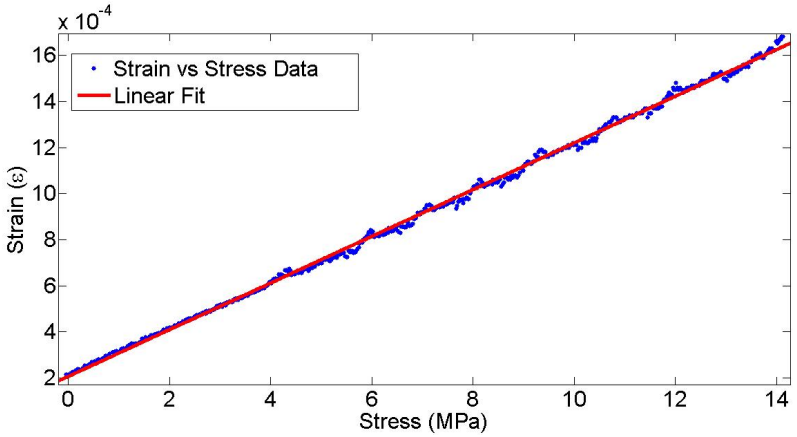

FIGURE 3.17: Strain vs Stress data for RTM-10

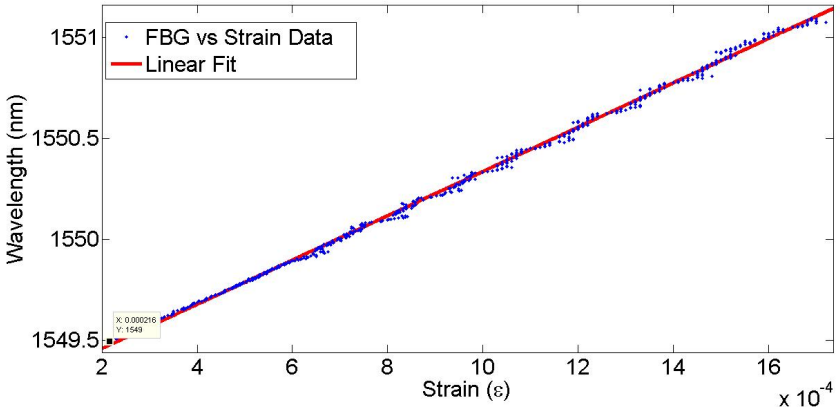

FIGURE 3.18: Wavelength vs Strain data for RTM-10

The average strain sensitivity of FBG sensors reported in literature is 1 nm/mϵ, which is in a good agreement with our results. One can note from both tensile test experiments that the fiber reinforcement type as well as the location of an FBG sensor between layers do not affect the strain sensitivity of the FBG sensors. These verification or calibration experiments enabled us to carry our research further toward structural health monitoring on composite materials with embedded FGB sensors inside composite material with the focus of damage detection elaborated in Chapter 4 and fatigue monitoring detailed in Chapter 5.

As stated previously, experiments on 3D specimens with embedded FBG sensors were also carried out. The cyclic loading experiments were conducted in Aeronautical Engineering Department at Istanbul Technical University (ITU) by using an MTS 322 test frame with MTS 647 hydraulic wedge grips, MTS FlexTest GT

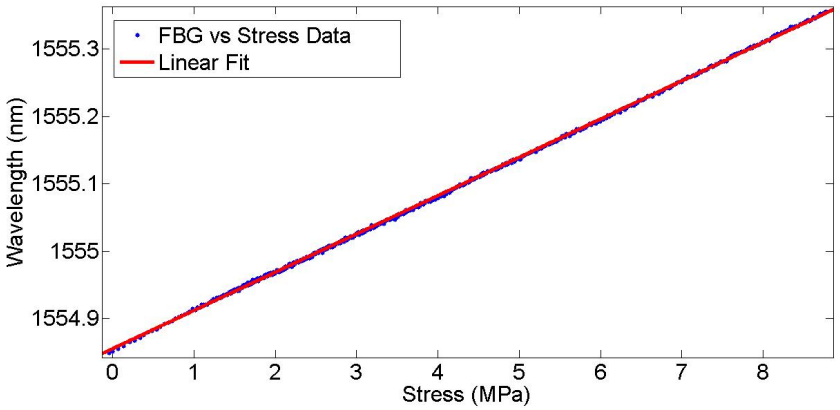

FIGURE 3.19: Wavelength vs Stress data for RTM-13

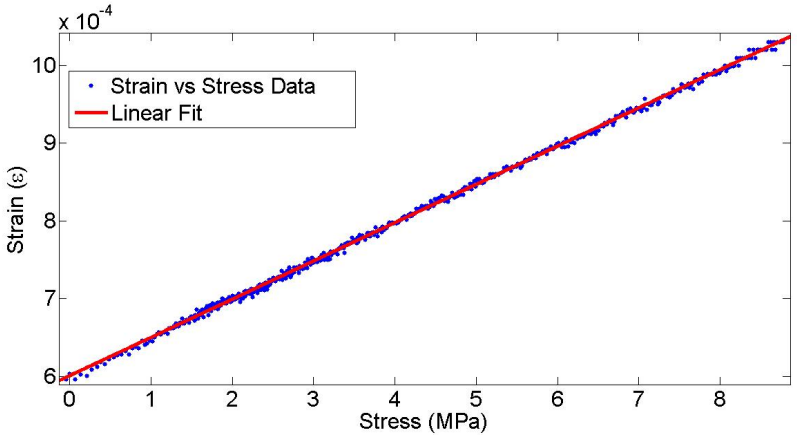

FIGURE 3.20: Strain vs Stress data for RTM-13

digital controller, and MTS Station Manager software. The square beams were cut in half creating two samples with an FBG sensor. The samples are presented in Figure 3.22. A fixture was designed and manufactured to connect the specimen to the MTS machine and solid drawing of the fixture is presented in Figure 3.23. In Figure 3.24, the sample with fixture is attached to the wedge of the MTS test frame.

The cyclic load was a 1Hz sinusoidal wave with peak to peak amplitude of 3kN in compression mode for 66000 cycles. The embedded FGB sensors were monitored with Micron Optics brand sm230 interrogator with the ENLIGHT program in 10Hz data acquisition rate. Figure 3.25 indicates the cyclic behavior in terms of wavelength of the embedded FBG for ten cycles.

These experiments validated our ingress/egress technique for 3D specimens as

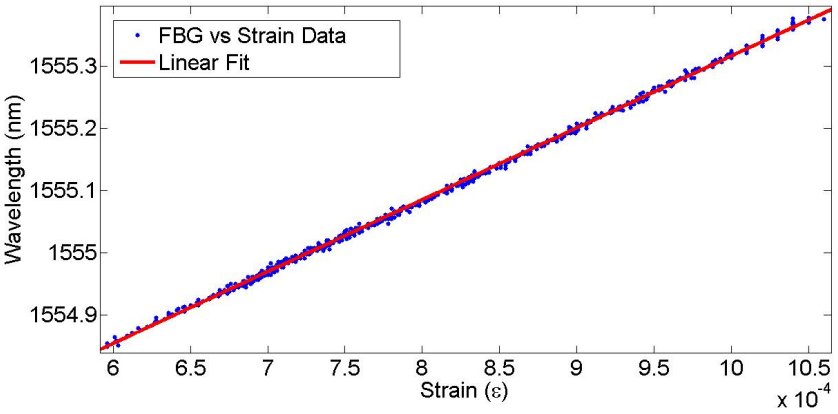

FIGURE 3.21: Wavelength vs Strain data for RTM-13

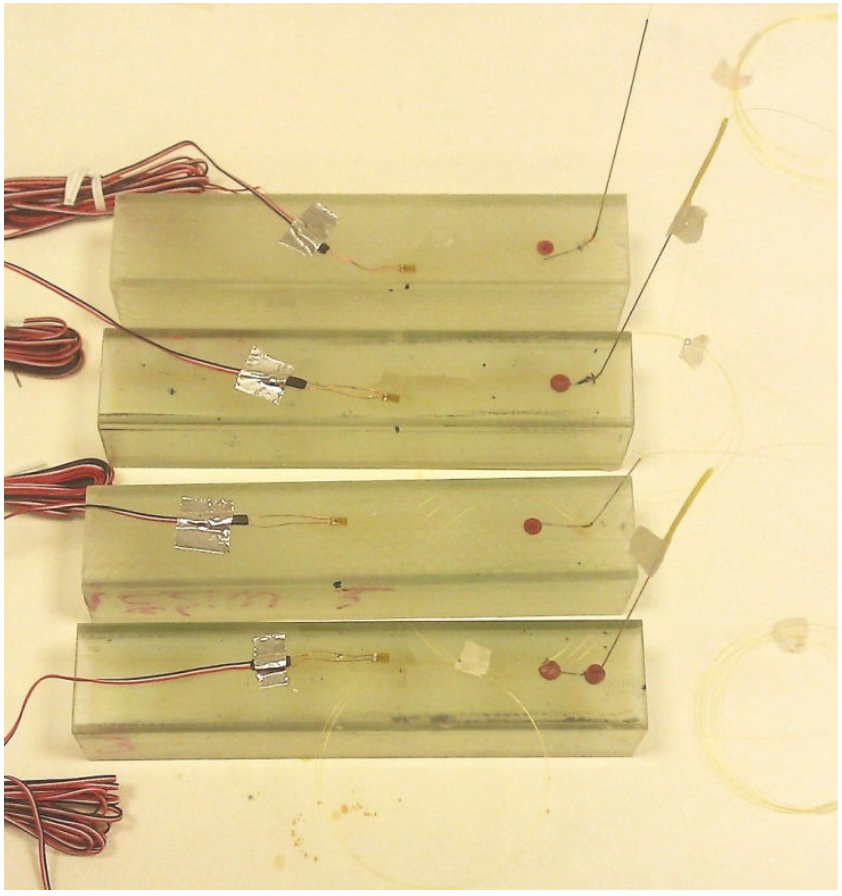

FIGURE 3.22: 3D samples that are used in cyclic loading

well. These cyclic loading experiments pointed out that 3D samples have very high strength compared to the 2D samples and performing fatigue experiments with 3D samples is not possible with the equipments possessed. Hence we have only performed fatigue experiments and remaining useful life prediction with 2D composites.

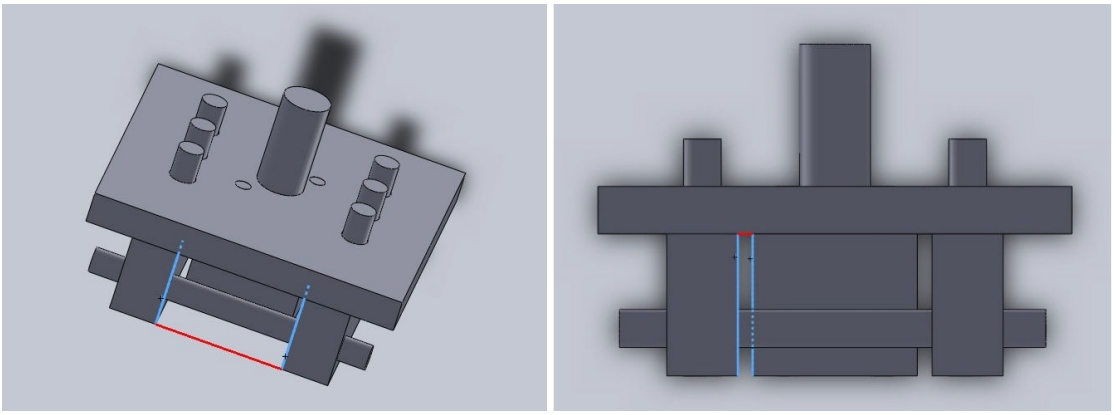

FIGURE 3.23: Solid drawing of the fixture that attaches samples to the wedge

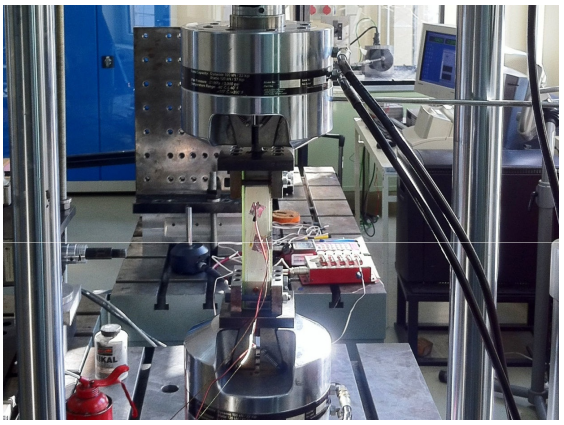

FIGURE 3.24: A sample attached to the MTS test frame

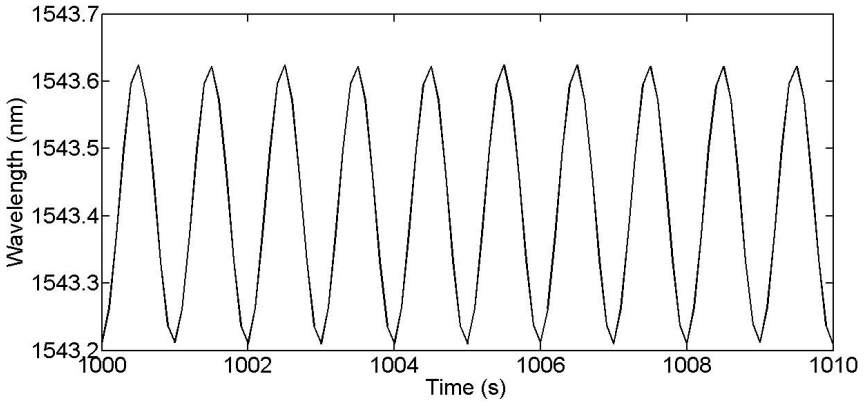

FIGURE 3.25: Cyclic behavior seen in wavelength of the embedded FBG sensor

3.4 Polarization maintaining fibers

As mentioned in Chapter 2, the polarization maintaining fibers transmit light in higher modes and an FBG sensor written on a PM fiber will reflect a spectrum with two Bragg wavelength peaks. Within the scope of this thesis work, we have

investigated the abilities and worthiness of PM FBG sensors in structural health monitoring.

3.4.1 Experimental system

An experimental system was designed and manufactured in order to explore the behavior of the polarization maintaining fibers in measuring transversal loading. An experimental setup for measuring transversal strain by PM FBGs presented in Figure 3.26.

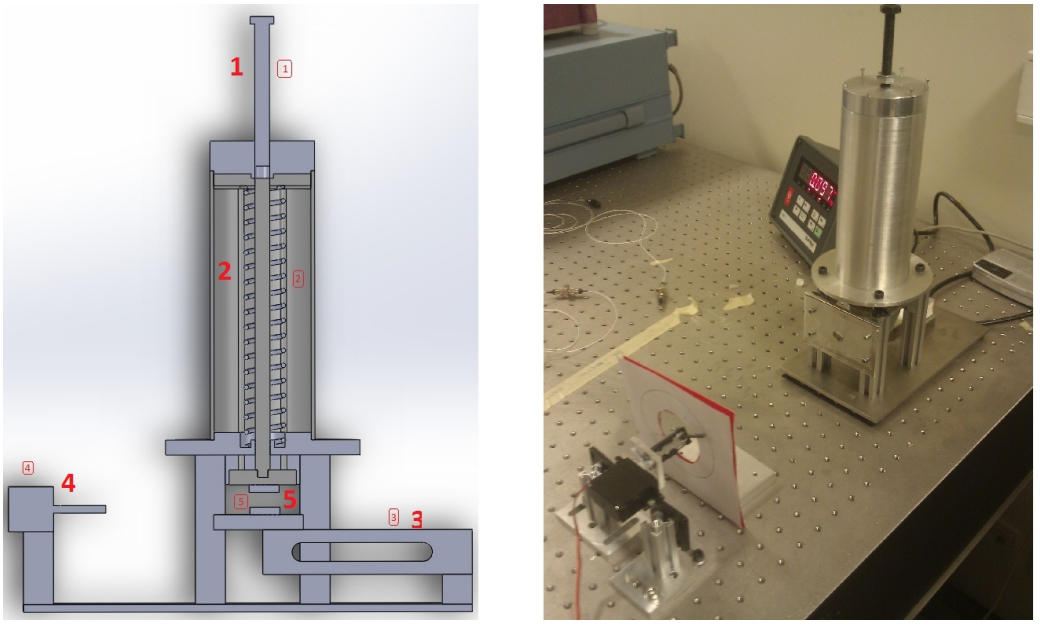

FIGURE 3.26: The solid drawing of the experimental system (left) and the experimental system (right)

In the solid drawing of the experimental system, the component **1** is a bolt which is used to apply transversal load to the PM FBG, the component **2** consists of a spring and a pin, the component **3** is a load cell with the sensitivity in the range of 1 gr up to 10kg, the component **4** is a servo motor by which the PM FBG can be rotated 360° around its axes and finally, the component **5** refers to the surface on which the PM FBG rests.

Load cell is a BAYKON brand single point type load cell with maximum capacity of 10kg. The indicator for the load cell is a BAYKON brand industrial type

electronic indicator with a standard RS232c port. The value of the load can be recorded continuously by connecting the indicator to a computer.

PM FBG sensors are monitored with interrogation circuit as shown in Figure 3.27 and the Bragg wavelengths of the slow and fast axes are tracked. Light generated by a broadband light source is sent to the PM FBG to excite both axes. Hence, reflected spectrum is a combination of FBG spectrum of both axes.

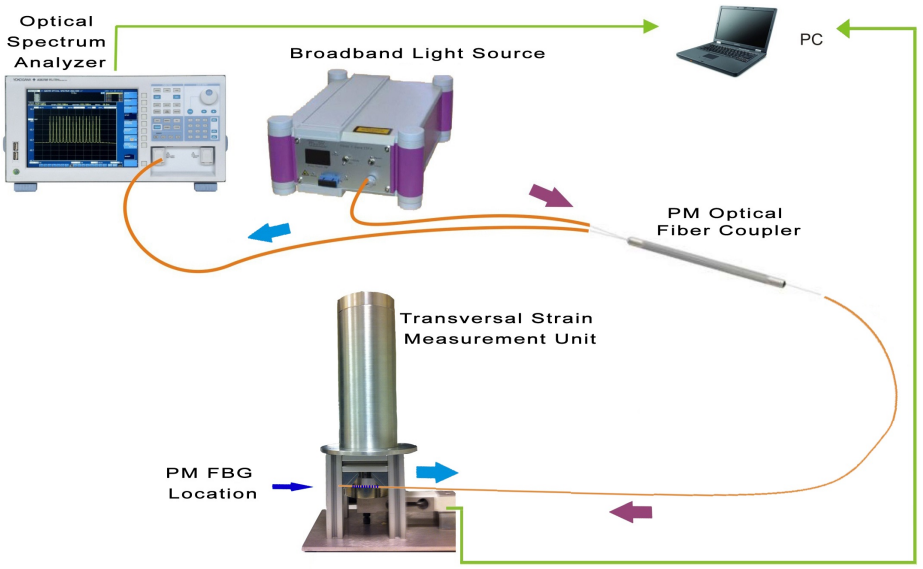

FIGURE 3.27: The interrogation circuit for tracking the Bragg wavelengths of slow and fast axes

3.4.2 Experimental procedure

PM FBG is placed on the surface which is located above the load cell. The application of the load is accomplished by the following the sequence of tasks; the bolt on the top of system is slightly turned whereby the spring is compressed and the base plate connected to the spring moves down to press on the PM FBG. The force applied on the PM FBG is measured by the load cell. Servo system enables us to turn PM FBG around its axes so that transversal load is applied at different angles with respect to the slow and fast axes.

3.4.3 Results and discussion

In the first set of experiments, the PM FBG sensor is rotated in steps of 30° and at each angle, 500gr constant force is applied. When the angle of rotation is 0°, the slow axis is aligned with the direction of the applied load and consequently, the slow axis sees maximum strain and the fast axis sees minimum strain. When the angle becomes 90°, the fast axis is aligned with the direction of the applied load and in turn, it sees the maximum strain while the slow axis sees the minimum strain. To be able to visualize above provided discussion, the results of experiments are plotted as a graph of the Bragg wavelength shifts of both axes and the angle of rotation in Figure 3.28. As the fiber optic cable is rotated between 0° and 90°, the change in the wavelength of the slow axis moves from negative values to positive values. The just opposite behavior is observed for the fast axis

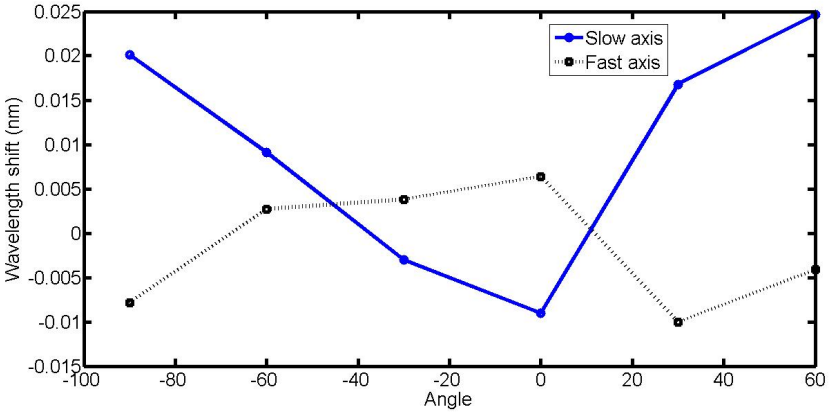

FIGURE 3.28: The shift of Bragg wavelengths of both axes in every angle

It should be noted that when the angle is 0° the strain induced by the transversal force is in compression mode. However, the fast axis sees tensile strain because fast axis is perpendicular to the slow axis. Consequently, the peaks of the both axes either get close to each other or move away from each other in the reflected spectrum. But they never move in the same direction as can be seen in Figure 3.29 and Figure 3.30.

In the second set of experiments, the transversal load in steps of 100gr up to 500gr is applied on the PM FBG at a constant angle of rotation of 60°. In Figure 3.31, the shifts in the Bragg wavelengths of the both axes are plotted against the applied

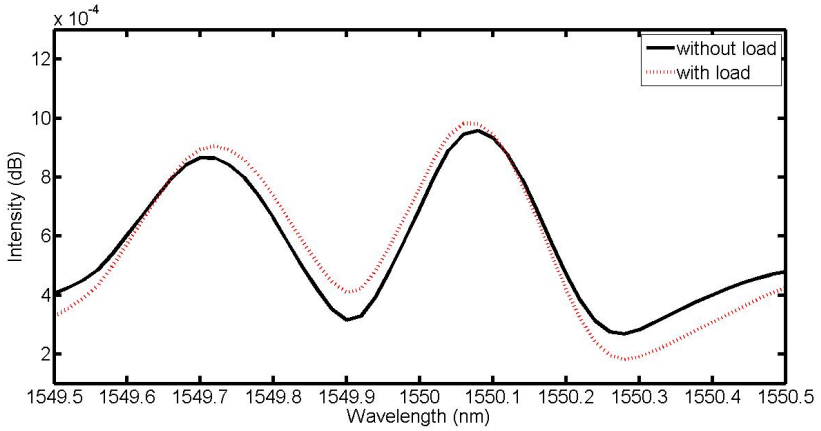

FIGURE 3.29: The Bragg wavelengths of both axes getting close to each other

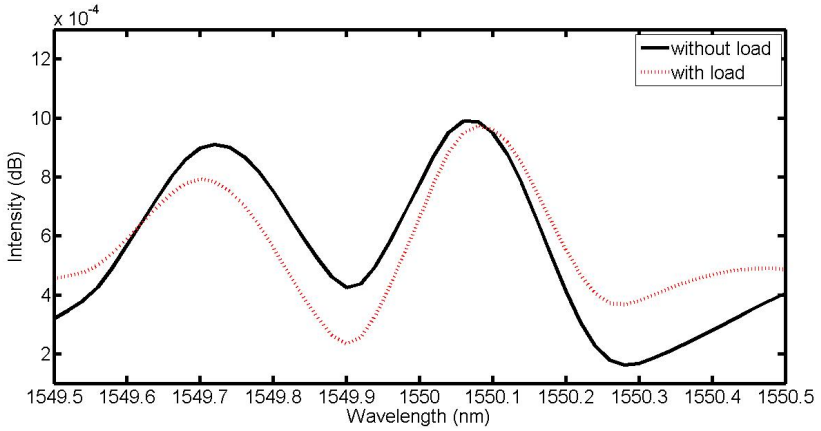

FIGURE 3.30: The Bragg wavelengths of both axes moving away from each other

incremental loads. As the transversal load is increased, the fast axis experiences increase in the tensile strain whereas the slow axis sees increase in the compression strain.

The slopes of both curves in Figure 3.31 give us the load sensitivity of both axes. The slopes of the slow and fast axis are calculated as $-4.1678 * 10^{-4} nm/kg$ and $5.4727 * 10^{-5} nm/kg$, respectively.

In conclusion, residual strain building up in composite materials in the course of curing process due to temperature differential, and non uniform cross section of the structure might be measured by a PM FBG sensor. However, the load sensitivity of PM FBG sensor is heavily dependent on the loading angle and in real applications, the angle of rotation of the sensor cannot be controlled precisely

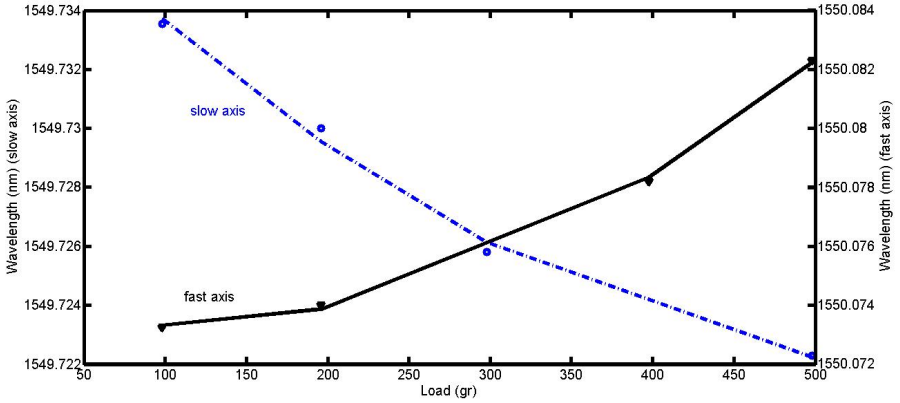

FIGURE 3.31: The shift of Bragg wavelengths of both axes against load

and repeatedly. Therefore, in this work, the PM FBG sensors are not embedded into the composite structures for transversal strain measurement.

Chapter 4

Damage Detection of Composite Materials

4.1 Introduction

Following the health monitoring of the composite structures with embedded FBG sensors in Chapter 3, in this chapter, the ability of the embedded FGB sensors for damage detection in composite materials are investigated [5]. The experimental setup and procedure are explained along with the method utilized for separating the temperature signal from the strain signal of the FBG sensor, which is hereafter referred to as temperature compensation. In the first section of this chapter, the cantilever beam setup is detailed. In the second section, the experimental procedure of loading and unloading the composite cantilever plate are described. Afterward, the temperature compensation of FBG sensor is demonstrated. At the last section, results of the damage detection experiments are presented.

4.2 Experimental setup

The composite plate used in this section is made of nine layers of biaxial glass fiber reinforcements (X 800 E05 800g/m2, manufactured by METYX) and the epoxy

resin system which is a mixture of ARALDITE LY 564 epoxy resin and XB 3403 hardener, mixed with the ratio of 100 and 36 parts by weight. The FBG sensor is located between the fourth and fifth layers of the composite. During the manufacturing of the composite plate, the curing process was monitored continuously using the embedded FBG sensor as it was mentioned in Chapter 3. The plot of the variation of the Bragg wavelength as a function of time is shown in Figure 4.1. The first sudden drop in the Bragg wavelength in Figure 4.1 is due to the contact of room temperature resin with the FBG in the preheated mold. Subsequently, the mold is heated to cure temperature of 50° Celsius resulting in a shift of the Bragg wavelength. The fluctuations in the figure correspond to a region where the temperature of the mold was set to the cure temperature. Since the cure process is exothermic, the released heat further shifts the Bragg wavelength. As the strength of the exothermic process diminishes, the water-cooling system in the RTM mold attempts to bring the temperature of the mold to the preset cure temperature. Given the presence of residual stress build up in the composite (due to various effects such as thermal gradients, shrinkage, and differentials in thermal expansion coefficients), the Bragg wavelength does not return to its original value. As the polymerization reaction nears completion, the shift in Bragg wavelength ceases. The region marked with two vertical lines corresponds to the curing of the epoxy system.

The composite plate manufactured with the dimensions of 305mm x 610mm x 3.5mm using the RTM system with the embedded FBG sensor was set up in a cantilever beam configuration as illustrated in Figure 4.2 with one end being fixed while the other end being free. The strain is measured using a quarter bridge Vishay 350Ω strain gage aligned vertically above the embedded FBG sensor and fixed on the surface of composite. The FBG sensor was interrogated using Micron Optic SM230 interrogator, and the strain gage was read using NI Signal Express with National Instrument data acquisition system explained in the Chapter 3.

Although our experiments were performed at room temperature, in industrial applications the ambient temperature always change. As it was mentioned in Eq.

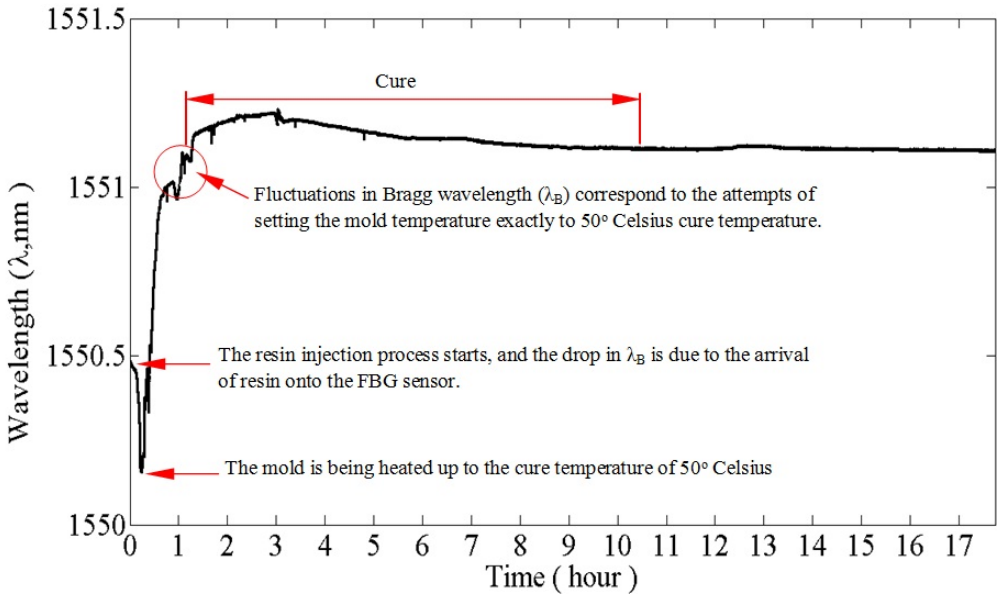

FIGURE 4.1: Bragg wavelength versus time for cure monitoring with the FBG sensor

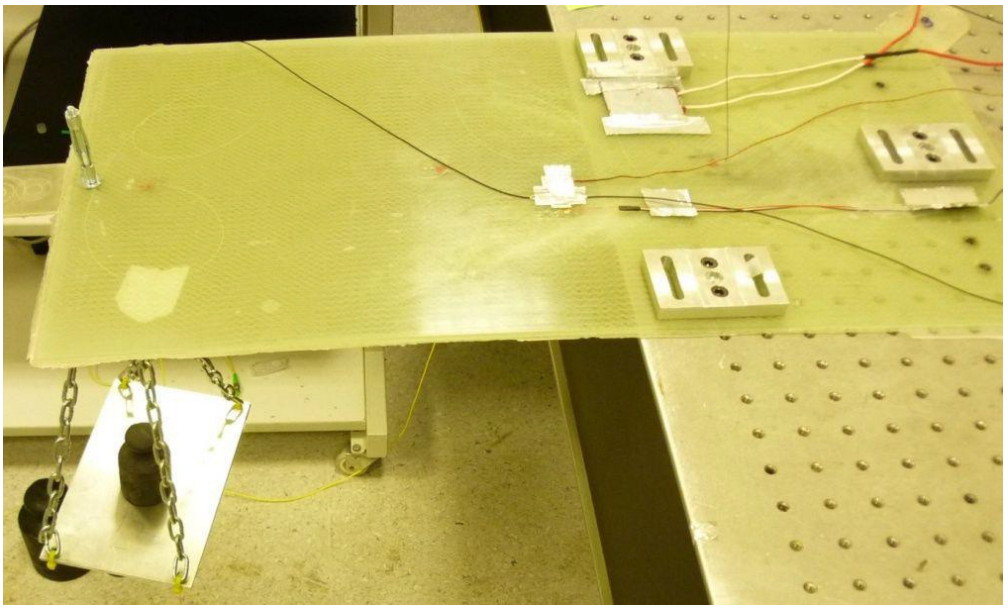

FIGURE 4.2: Bragg wavelength versus time for cure monitoring with the FBG sensor

2.4, FBG sensors are sensitive to the temperature change. Hence the temperature effect should be eliminated in order to obtain the wavelength shift that is only resulted from the strain. In this regard, a heat patch which has dimension of 10mm x 10mm was placed under the embedded FBG in the composite plate. Furthermore, a Micron Optics FBG temperature sensor is patched on top of the embedded FBG in the composite plate. This FBG temperature sensor is placed

inside a tube. Although it senses the temperature change, optical fiber slides inside the tube when strain applied to the fiber.

4.3 Experimental procedure

The experimental procedure is a cantilever beam experiment as in Figure 4.3. To create strain on the composite panel, load was applied to the free end in steps of 0.5 kg up to 3.5 kg. At each load, the strain and the Bragg wavelength were recorded. The temperature change was carried out by changing the applied voltage to the heat patch.

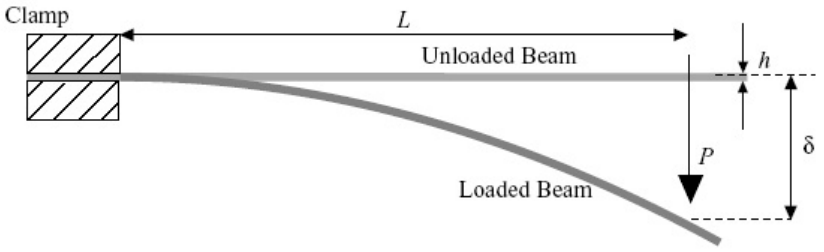

FIGURE 4.3: Schematic of the cantilever beam experiment

For damage detection of composite under controlled environment, artificial defects were created in the composite panel manufactured. The composite plate was drilled at 7 cm away from the FBG sensor location as illustrated in Figure 4.4. The diameter of the hole is 3 mm and then the hole size was subsequently enlarged to 6 mm.

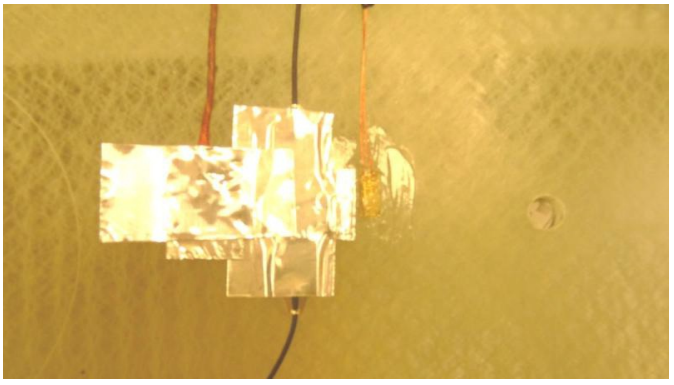

FIGURE 4.4: The picture of damaged composite panel with a hole diameter of 6 mm

4.4 Temperature compensation

Temperature compensation was conducted by doing three experiments. First only strain was applied to the system. In the second experiment, temperature of the system is altered without any loading. In the last experiment, strain was applied to the system along with the heating of the system. In the first experiment, the strain sensitivity of embedded FBG sensor was calculated. In Figure 4.5, the wavelength shift of both embedded FBG sensor and FBG temperature sensor is presented in black and red, respectively. As it can be seen from the figure, the FBG temperature sensor is not affected by the load applied to the composite.

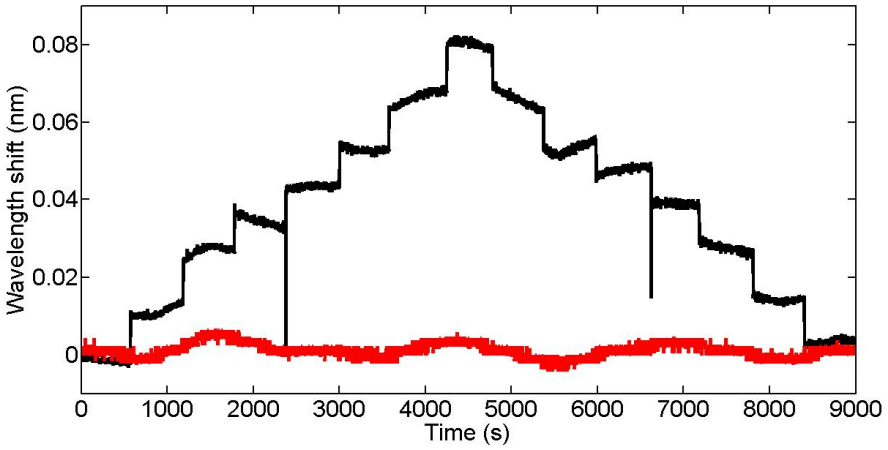

FIGURE 4.5: Wavelength shift of embedded FBG(black) and FBG temperature sensor(red) with only strain applied

To be able to determine the strain sensitivity of the FBG sensor, the Bragg wavelength is plotted as a function of the measured strain, and the slope of this linear plot in Figure 4.6 is determined to be 0.08 pm/ϵ. This very low value is a result of embedding the FBG close to the neutral axis of the composite. The very high sensitivity of free and bare FBG enables measurements even close to neutral axis.

In the second experiment, the temperature sensitivity of both embedded FBG sensor and FBG temperature sensor was calculated. As mentioned above, the temperature of the composite is changed by tuning the applied voltage on the heat patch. The division of the change of the Bragg wavelength over Bragg wavelength is plotted against temperature in Figure 4.7. The temperature sensitivity

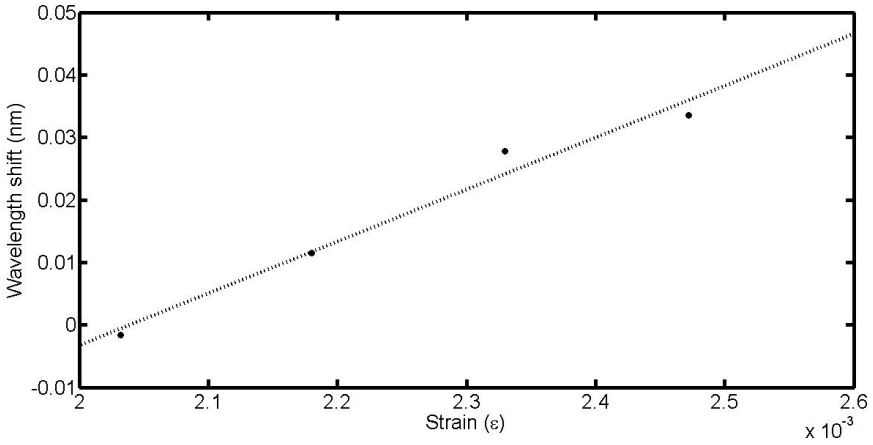

FIGURE 4.6: Calibration of the FBG with the surface mounted strain gage

of the embedded FBG sensor and FBG temperature sensor is calculated as 3.19 pm/Celsius and 4.11 pm/Celsius, respectively.

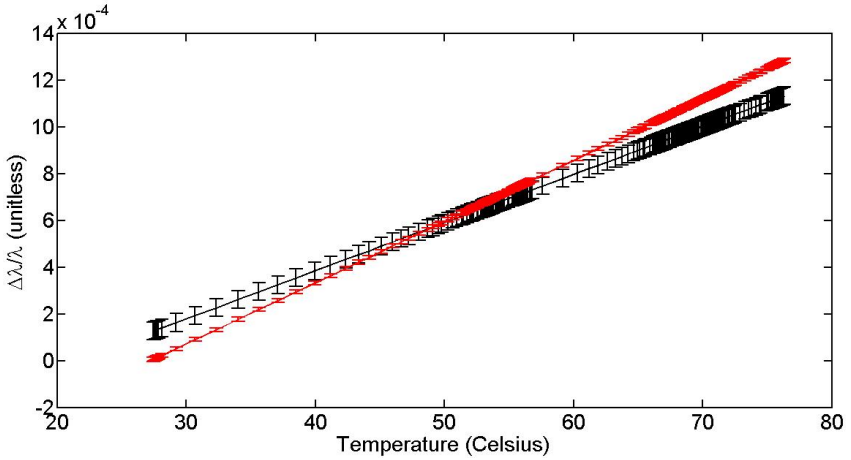

FIGURE 4.7: Wavelength shift of embedded FBG(black) and FBG temperature sensor without any strain

In the last experiment, temperature compensation is performed via putting the sensitivity factors into the Eq. 2.9. The composite plate is heated to 109° Celsius and it was loaded while the temperature was changed between 105° Celsius and 109° Celsius. In another words, the embedded FBG sensor was exposed to strain while temperature is altered. With using Eq. 2.9, the wavelength shift that is only resulted from the strain is calculated from the wavelength shift data which accomodate effects of both strain and temperature. Afterwards, the calculated wavelength shift is compared to the wavelength shift data from the first experiment in which only strain was applied. As it is represented in Figure 4.8, the calculated

wavelength shift correlates with the wavelength shift that occurred due to the strain change. This exhibits that with this method temperature effect on the embedded FBG sensor can be compensated successfully.

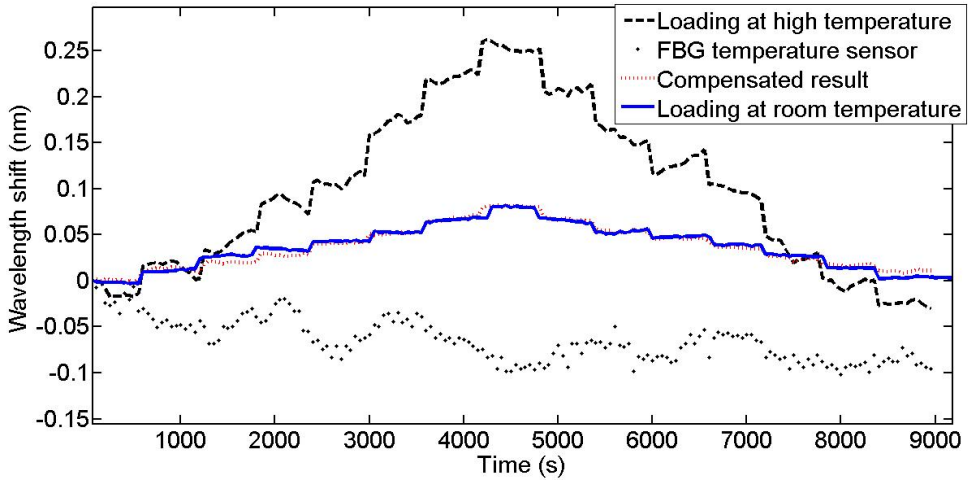

FIGURE 4.8: Graph of temperature compensation experiment

4.5 Results

As it was explained above, the composite plate has been drilled first for 3mm and then for 6mm. In the meantime the Bragg wavelength of the embedded FBG sensor was monitored for healthy and damaged plates, as given in Figure 4.9. As can be seen from the figure, the wavelength shift of the embedded FBG sensor has increased after drilling a hole through the composite structure, and it increases more for a larger hole. This change in the Bragg wavelength is due to the release of the compressive residual stress accumulated within the composite structure because of the curing process.

The damaged composite plate with the hole size of 6 mm was also employed as a cantilever beam, and the loading experiments were repeated and compared with the sound structure. The results of the wavelength shift of the embedded FBG sensor in Figure 4.10 showed that damage near FBG sensor causes the wavelength shift to decrease for the given load. This is due to the fact that the presence of damage alters the strain distribution in the structure. Thus, the damage can

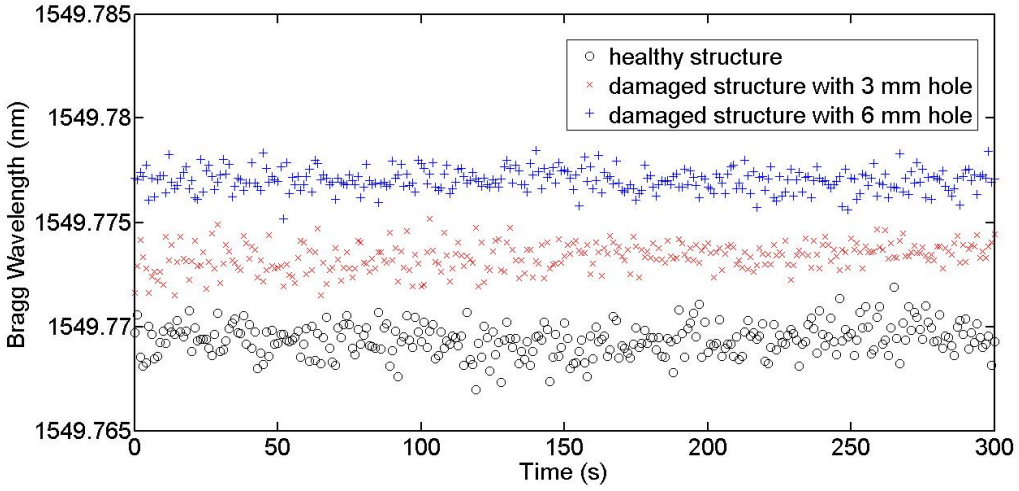

FIGURE 4.9: The Bragg wavelength of the embedded FBG sensor of sound structure and damaged structure

be detected when the measured strain differs significantly from that of a healthy structure, thereby allowing one to be able to monitor the structural health of composite components under service conditions. This can be more readily seen in Figure 4.11 where the wavelength shift of the embedded FBG sensor is plotted as a function of the applied load.

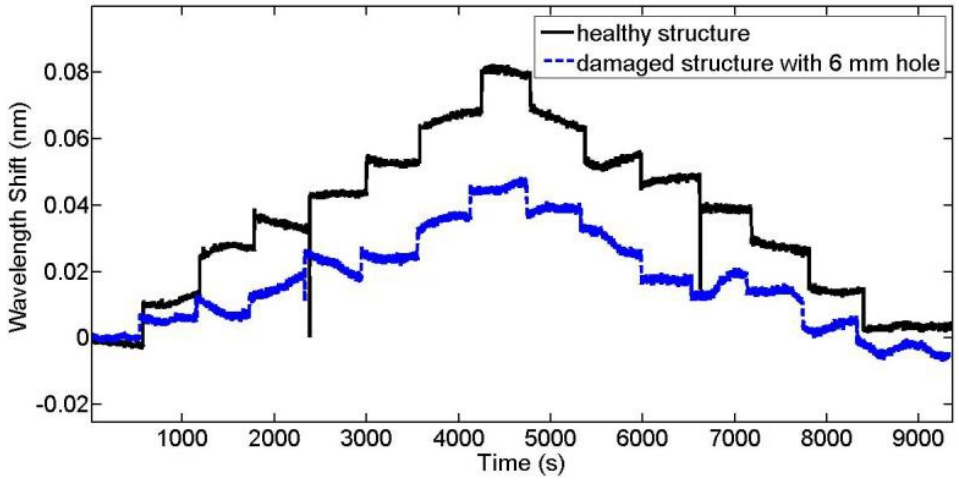

FIGURE 4.10: The wavelength shift over time in cantilever beam experiments with and without damage.

With damage detection experiment, it is revealed that the embedded FBG sensor can detect the presence of damage formation in the structure. Following detecting the presence of the damage, the composite material will be tested with NDT methods to asses the damage throughly. Additionally, this validation makes the FBG

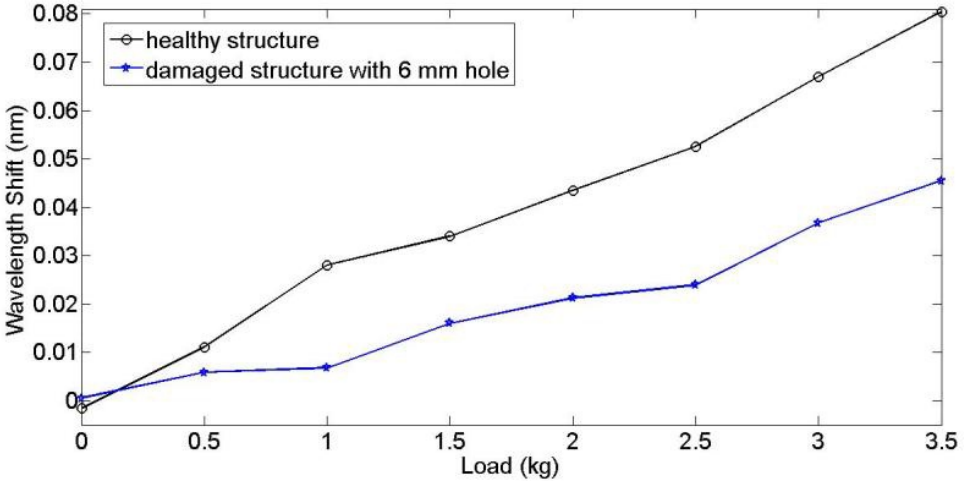

FIGURE 4.11: The wavelength shift versus the applied load in cantilever beam experiments with and without damage

sensors very good candidate for fatigue monitoring because structures deteriorate in fatigue. Hence embedded FBGs in our composite materials will be able to sense the damages occurred in the fatigue and predict the remaining useful life. The fatigue monitoring and its prediction results is presented in the next chapter.

Chapter 5

Fatigue Monitoring and Remaining Useful Life Prediction

5.1 Introduction

In this chapter, the results of the novel technique for prediction of the remaining life of composites under fatigue loading using embedded FBG sensors which was detailed in Chapter 2 is presented. Two types of composite materials were employed in the fatigue monitoring, namely glass and carbon fiber composites.

5.2 Testing equipment

All tests were performed on an MTS 322 test frame with MTS 647 hydraulic wedge grips using an MTS FlexTest GT digital controller with MTS Station Manager software. Load and displacement data was collected with a built in load cell, model: MTS 661.20F-03 and linear variable differential transformer (LVDT), respectively. Strain data was collected with an axial extensometer, model: MTS 634.25F-24. All FBG data was collected with a Micron Optics SM230 interrogator using Micron Optics Enlight software. Temperature data was collected with a K-type thermocouple using a National Instruments NI SCXI-1314 DAQ card in

a NI SCXI-1000 chassis with LabVIEW software. The fiber Bragg gratings used in the experiments were $10mm$ long with a center wavelength of either 1555 or $1565nm$ supplied by FiberLogix. All data is acquired at a sampling rate of $100Hz$.

5.3 Test procedure

At first material properties are characterized with specimens without embedded FBG sensors. With the characterization experiments, the fatigue coefficients are determined (a and b from Equation 2.19) which gives the relation between strain energy release rate and strain. Before fatigue experiments, the ultimate tensile strain, ε_{ult}, of the material is determined via static testing. With the ε_{ult} value, fatigue tests were performed at different strain levels. From those fatigue tests a and b values were calculated by plotting strain energy release rate as a function of strain. Following this step, experiments with embedded FBG sensors were conducted. For this study, a number of fatigue tests at each of the following strain amplitudes ($\varepsilon_{max}/\varepsilon_{ult}$): 0.8, 0.75, 0.7, 0.6, 0.5 and 0.4 are performed including two fatigue tests with specimens containing embedded FBGs. A static test is also performed to determine the ultimate strain of the embedded FBG.

Glass fiber composites do not conduct heat quickly as metallic materials. Therefore autogenous heating constitutes a problem during fatigue testing as the FBG sensors are sensible to the temperature change. Generally a fatigue loading frequency of 1-4Hz for glass fiber has been used with no adverse effect. All our experiments were performed with frequency of $4Hz$. Additionally, a thermocouple was fastened to the surface of the specimen to monitor any temperature increase due to autogeneous heating. Temperature sensitivity of embedded FBG sensors were measured by putting the specimens inside an oven. The oven was heated for different temperatures as $30°C$, $40°C$, $50°C$ and $60°C$. An average temperature sensitivity of $0.031nm/°C$ was found for embedded FBG sensors.

All fatigue tests are constant amplitude strain, tension-tension sine wave tests. The maximum and minimum load and displacement is recorded via MTS Station

Manager software. The extensometer of the MTS machine did not offer strain controlled testing, therefore the displacement value corresponds to the intended strain level is measured with a calibration experiment and used in fatigue testing. The specimen is loaded to the machine and desired value of stress is applied to the specimen for two cycles. At the end of the second cycle, there is a residual displacement sensed by the LVDT. This zero offset is caused by the wedge grips tightening and the specimen slipping slightly before the full clamping force is realized. Although the zero offset value is small, it is accounted for and this value is substracted from the maximum displacement from the second cycle. Additionally, the strain is measured with the extensometer as well. Subsequently, the fatigue testing procedure begins by entering the maximum displacement value from the calibration process and the minimum displacement value.

5.4 Fatigue monitoring of glass fiber composites

Experimental validation involves producing fatigue specimens with and without embedded FBG sensors, testing specimens without embedded FBG sensors to characterize the material then testing and applying the failure model to specimens that contain embedded FBGs. Due to the nature of the fatigue experiments, this work is conducted by our group and the results have been submitted to Journal of Intelligent Material Systems and Structures on June 26, 2012 [32].

5.4.1 Specimen preparation

Specimen preparation has a large impact on the test results of both static and fatigue tensile testing. It is very important that they are prepared with the utmost care in a consistent manner. It is a tedious and time-consuming process yet very important for producing accurate and reliable test results. The RTM apparatus in our lab which was described in Chapter 3 is used to produce flat panels $610mm$ x $305mm$ x $3.5mm$ that are processed into specimens for fatigue testing.

The laminate selected for this research is $[0/90]_{6S}$ E-glass fiber with epoxy resin. The fiber used is Metyx LT300 E10A 0/90 biaxial E-glass stitched fabric with $161gsm$ in the 0° orientation and $142gsm$ in the 90° orientation, summing to $313gsm$ total. The selected resin is Araldite LY 564 epoxy resin with XB 3403 hardener produced by Huntsman Corporation. The panels undergo an initial cure at $65°C$ for 24 hours with a post cure at $80°C$ for 24 hours. Three panels were produced for this study and processed into specimens. Specimens were named with the convention #-##; with the first number indicating the panel they were cut from and second indicating the order in which they were cut. Panel numbering starts at #2 as panel #1 was used for preliminary investigation.

Each panel produces ∼30 specimens. A tabbing material composed of $1.5mm$ thick, plain weave E-glass non-crimp fabric/epoxy with a ∼20° angle on one edge is bonded with West System 105 epoxy and 205 hardener thickened with milled glass fiber with a bond-line thickness of $0.7mm$. The panels are cut on a water-cooled diamond blade saw and the edges polished up to 400 grit sandpaper. The final dimensions of the specimens are $280mm$ x $15mm$ x $3.5mm$ with a $160mm$ gage length. The length of the specimen is aligned with the 0° fiber orientation. Figure 5.1 represents solid drawing of a specimen with an embedded FBG sensor.

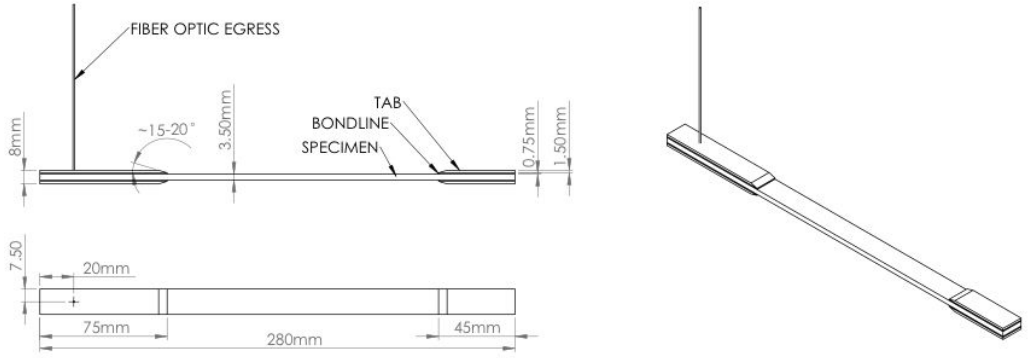

FIGURE 5.1: Solid drawing of a fatigue specimen

A special fixture is required to grip the specimen such that the fiber optic ingress location is not under load. The fixture consists of three steel plates, a bar and a pin. Two plates are clamped across either side of the specimen with bolts. One plate has a slot that allows the fiber to egress from the composite. The plates

are screwed into the third plate that has a cylindrical pin that interfaces with the machine grips. A stiffening bar is located across the slot to reduce deflection when the bolts are tightened. The solid drawing of the fixture with a specimen inside is shown in Figure 5.2.

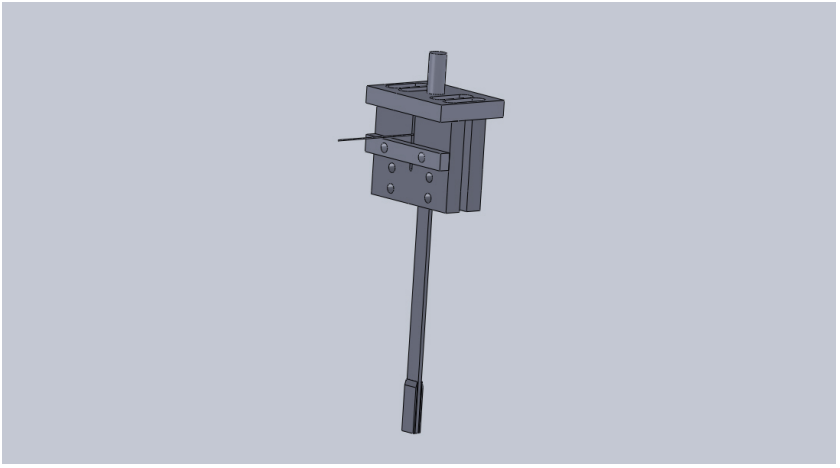

FIGURE 5.2: Solid drawing of the special fixture with a specimen

Once cut to size, it is very important that the edges of the specimens be smooth and free of gouges. Any abnormality or unevenness along the surface can act as a stress riser/failure initiation point and have an adverse impact on the test results; a mirror finish is desirable. The specimens were sanded with 280, 320 and finally 400 grit sandpaper by placing the paper on a large glass surface and oscillating the specimens back and forth by hand. The glass surface ensures that the specimen edges are flat and consistent. The initial sanding with 280 took the longest, as this is the stage where any unevenness was removed. Water with a little bit of hand soap was sprayed on the specimens during sanding to control the dust and wash it away as well as to provide lubrication.

Once the specimens were prepared, all of their dimensions were measured and recorded in a spreadsheet. The thickness and width was measured in three places and the average of these properties was used for calculations.

5.4.2 Material characterization test results

Ultimate tensile strain, ε_{ult}, is determined by 11 static tests. The ultimate stress and strain were found to be $318.75MPa$ and $16.31m\varepsilon$. The minimum stress applied to the specimen during fatigue testing is chosen as $27.6MPa$ which is close to that used by Natarajan [47].

After determining the ultimate stress and strain values, fatigue testing of the composite materials was carried out at different strain levels. From the load data, expended strain energy per cycle is calculated and plotted. The plot of an expended strain energy per cycle was represented in Figure 2.7. The graph of the expended strain energy per cycle is plotted as a function strain level in Figure 5.3.

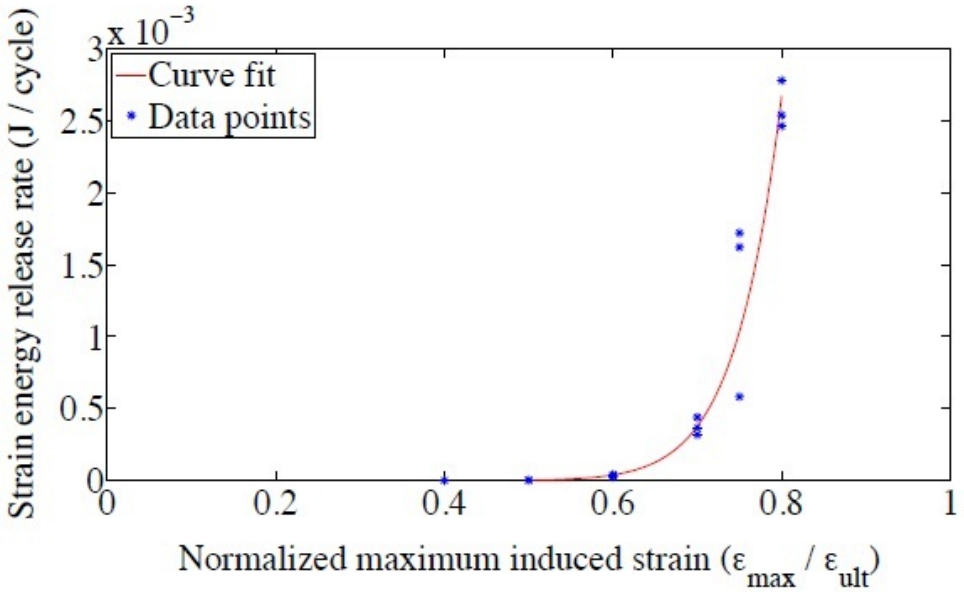

FIGURE 5.3: Variation of energy release rate

Linear regression was used to obtain the energy release rate (dU/dN) throughout the linear region. The average energy release rate and ratio of U_f/U_0 for various levels of induced strain are presented in Table 5.1. The ratio U_f/U_0 (energy at failure, U_f (90% of total cycles) to initial energy U_0) is significant as it is used in the prediction of the remaining cycles in Eq. 2.22. The average value of $r = U_f/U_0 = 0.856$ was used for predictions.

$\varepsilon_{max}/\varepsilon_{ult}$:	Energy Release Rate (J/cycle):	$r = U_f/U_0$:
0.4	8.705E-08	0.799
0.5	3.337E-06	0.826
0.6	3.352E-05	0.855
0.7	3.736E-04	0.885
0.75	1.307E-03	0.901
0.8	2.592E-03	0.917

TABLE 5.1: Fatigue test data for glass fiber composites

The energy release rate was plotted vs. normalized induced strain, Figure 5.3. This data was averaged, plotted and fit to a power law curve to obtain the values for fatigue coefficients a and b, of 14.67 and 0.070595, respectively. With a and b determined, the fatigue life could be predicted using Eq. 2.22. The experimental and predicted results are plotted as an $\varepsilon - N$ curve in Figure 5.4. The number of experimental and predicted cycles to failure (N_f) and percent difference is shown in Table 5.2.

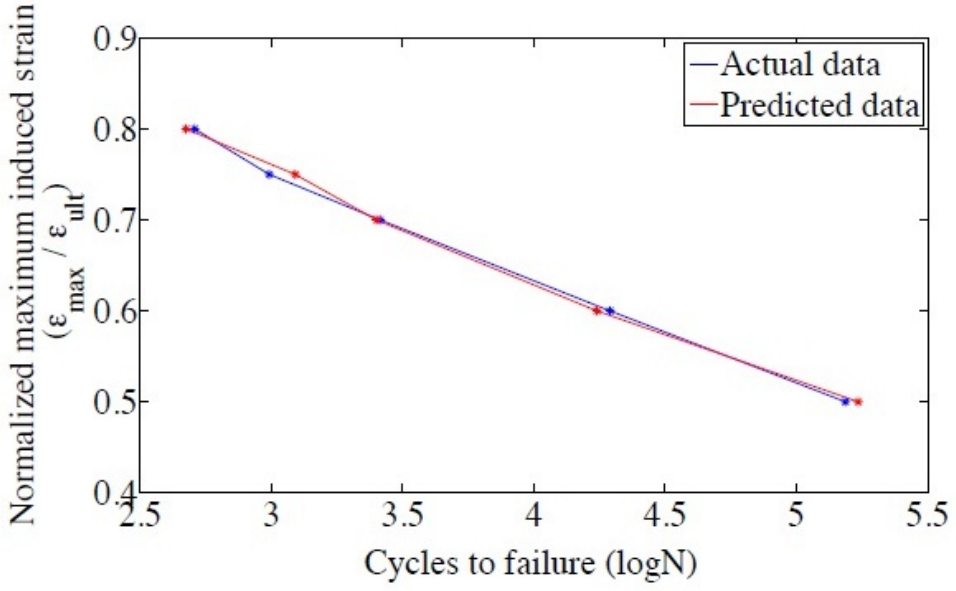

FIGURE 5.4: Predicted results as an $\varepsilon - N$ plot

5.4.3 Embedded FBG test results

One problem that was immediately apparent was that as the FBG was strained, the reflected spectrum broadened, reduced in magnitude and split into multiple

$\varepsilon_{max}/\varepsilon_{ult}$:	Experimental N_f:	Predicted N_f:	Difference (%):
0.5	154108	185132	20.13
0.6	19510	17475	-10.43
0.7	2597	2389	-8.00
0.75	1233	982	-20.34
0.8	510	428	-16.17

TABLE 5.2: Fatigue life prediction results

peaks making it difficult to accurately track. This is due to the uneven strain field caused by matrix cracking and the fiber reinforcement arrangement as documented by Takeda [60], [61], Shin [59], Okabe [49], Yashiro [73] and others. The peak splitting resulted in an inaccurate measurement of the strain magnitude, either greater or less than the actual strain. As the peak split, the tallest peak would move to either side of the Bragg wavelength. The interrogator algorithm would track this peak rather than the center wavelength thus resulting in inaccurate strain values.

The reduction in magnitude also presented a problem. One of the settings of the interrogator software is the threshold of the magnitude of the reflected spectrum. The threshold must be set high enough to eliminate noise but not so high that the FBG reflected spectrum is excluded. Under low strain there was not enough of a reduction in magnitude to drop below the threshold, however as the strain increased towards the upper limits the magnitude reduced and in some cases dropped below the threshold causing the interrogator to momentarily lose the signal. This resulted in a number of data points that were recorded as 0. When the peaks were extracted from the full waveform data, missing peaks were given a value that was determined by interpolating between the neighboring peaks. The acquired signal from Specimen 3-1 for five second intervals of the fatigue test is shown at the beginning in Figure 5.5 and at the end in Figure 5.6. The blue lines show the acquired data at an acquisition rate of $100Hz$ while the red circles indicate the peaks and troughs of the data that were extracted from the full waveform.

The surface temperature of the specimens that was monitored during the tests was converted into a wavelength value ($\Delta\lambda_B$) using the temperature sensitivity

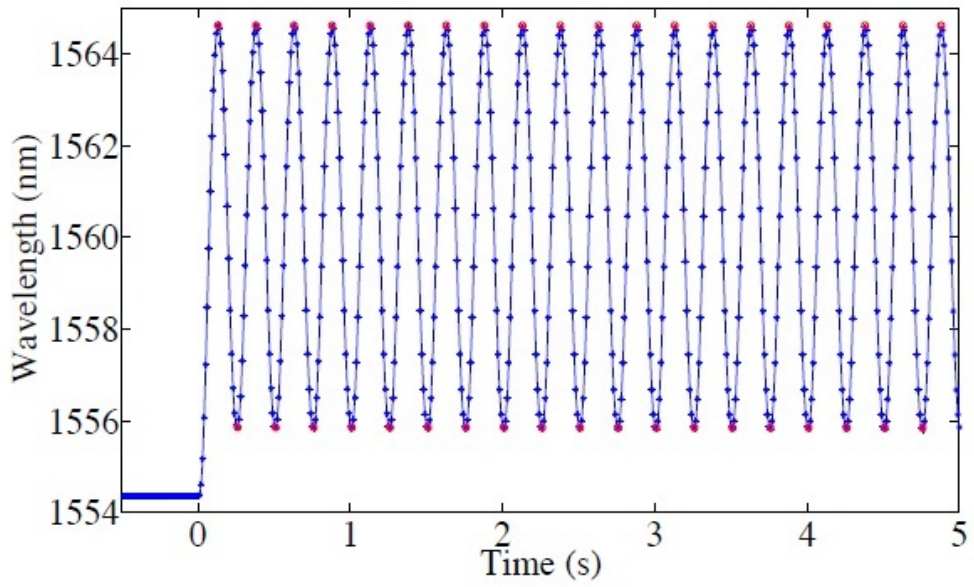

FIGURE 5.5: Wavelength vs. time for five second intervals at beginning of the test

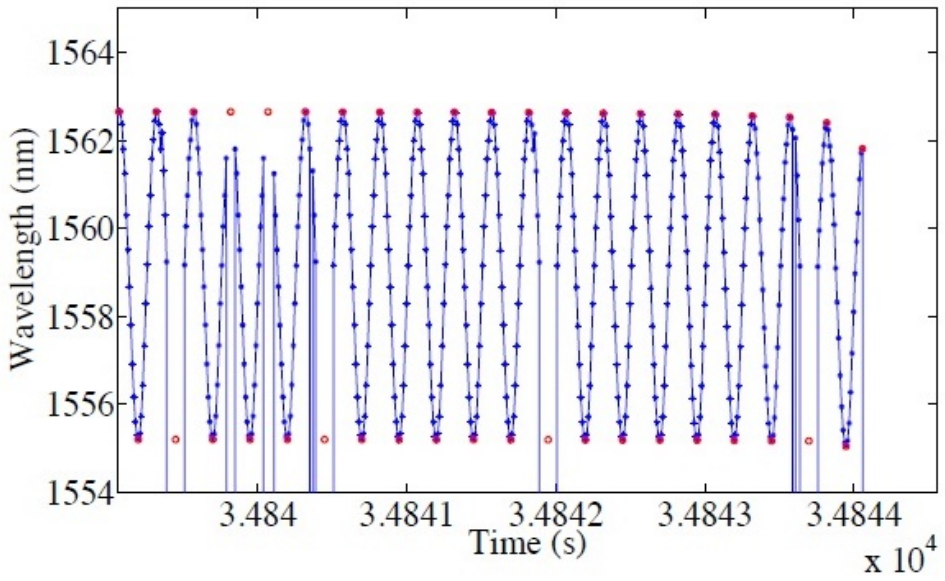

FIGURE 5.6: Wavelength vs. time for five second intervals at end of the test

described earlier. The wavelength change due to temperature was subtracted from the FBG data.

The first test performed was a quasi-static tensile test to determine the ultimate strain level of the embedded FBG in Specimen 2-2. This information would provide a range of strain levels to conduct the fatigue tests.

Figure 5.7 shows a plot of strain measured with an extensometer on the left vertical axis and FBG wavelength on the right vertical axis vs. stress. Both strain and wavelength follow a linear increase until roughly $160MPa$ when there is a small jog in the FBG signal. This is likely due to the FBG reflected spectrum splitting and the peak moving to the lower range of the spectrum. After the jog the increase in the signal remains linear as expected. The strain level measured by the extensometer when the fiber optic broke was $10.323m\varepsilon$ while the FBG read $10.039m\varepsilon$ due to the shift. It is also worth mentioning that a loud 'ping' noise was heard when the fiber optic broke/signal was lost.

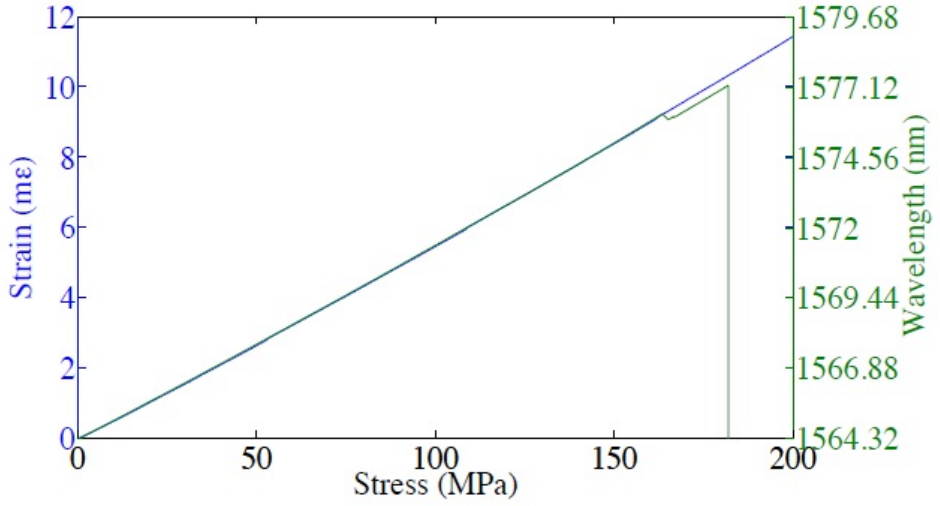

FIGURE 5.7: Wavelength and strain vs. stress

Before fatigue tests began, a simple strain characterization test was performed to determine the strain sensitivity of each specimen by straining it and monitoring the Bragg wavelength, displacement and strain in the specimen. FBG sensitivities of $1.2596nm/m\varepsilon$ and $1.2691nm/m\varepsilon$ were obtained for Specimen 3-1 and 4-2, respectively. The conversion from LVDT acquired displacement to strain was also obtained.

Specimen 3-1 was tested at a maximum induced strain of $0.5^{*}\varepsilon_{ult}$. Figure 5.8 shows the strain data vs. cycle number throughout the test. The blue line indicates LVDT acquired displacement data and the red line indicates FBG wavelength data. Both data sets are converted to strain for application to the prediction

technique. The data measured with the LVDT shows a steady constant strain throughout the entire test as expected. The FBG data however, initially shows a sharp increase due to autogeneous heating followed by a nonlinear decrease which leads to a linear decrease until roughly 13.5 x 10^4 cycles when it exhibits a sharp nonlinear decrease until failure. This shows the same trend as the load and is likely due to the break down of the composite resulting in a non-uniform strain field that causes the FBG peak to broaden.

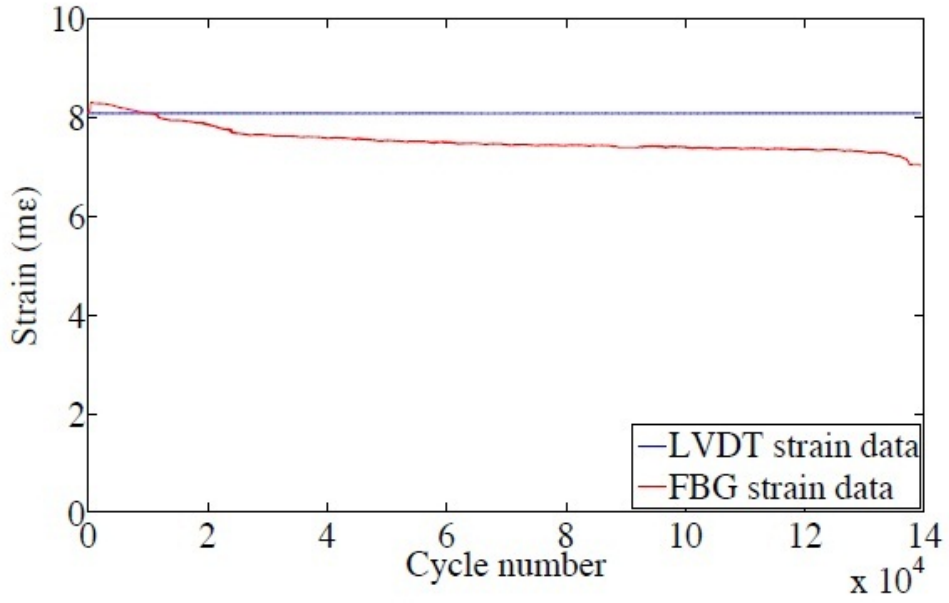

FIGURE 5.8: Strain data for Specimen 3-1

Figure 5.9 shows the prediction results from the data presented on the left along with the actual failure data. The prediction is made at every cycle based on data from the LVDT and FBG in blue and red, respectively. Since the LVDT data is constant, the predicted number of remaining cycles remains linear with a constant offset from the actual data. The error in these results is a function of the accuracy of the prediction method and experimentally determined fatigue coefficients from Eq. 2.19. The predicted results are within 27% of the actual results at the beginning of the test. This larger than average difference compared to the average results shown in Table 5.2 can be attributed to the statistical variation in the material properties from specimen to specimen. The predicted results from the FBG data however, are not as accurate due to the reduction in

magnitude of the strain signal. Since the prediction formula is based on a power law, a small variation in measured data can result in a large discrepancy between actual and predicted results. For the first 2 x 10^4 cycles the FBG prediction results are quite close to the LVDT prediction before they drift away to an unreasonable value.

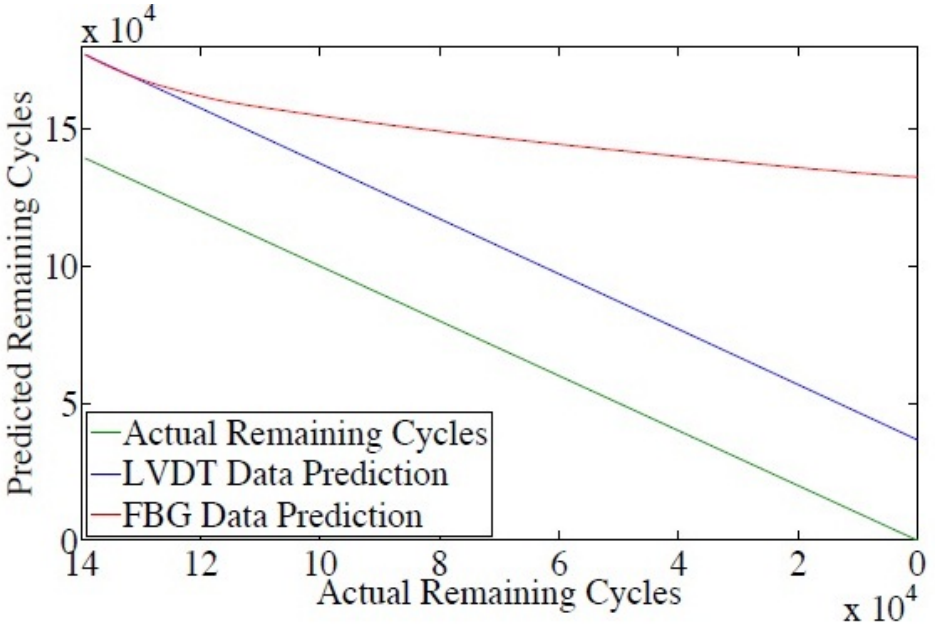

FIGURE 5.9: Prediction of remaining cycles for Specimen 3-1

In an attempt to subject the embedded FBG to a lower ε_{max} to obtain a more accurate signal, Specimen 4-2 was tested at a maximum induced strain of $0.4^*\varepsilon_{ult}$. Figure 5.10 shows the strain data vs. cycle number throughout the test. The blue line indicates LVDT acquired displacement data and the red line indicates FBG wavelength data. Clearly the signal from the FBG is much closer to that measured by the LVDT than for Specimen 3-1. Naturally this results in a more accurate prediction of the remaining cycles as shown in Figure 5.11.

5.4.4 Remarks

The quasi-static test of the specimen with an embedded FBG showed that the ε_{max} of the embedded fiber optic is $\sim 10m\varepsilon$. The data also demonstrated the peak

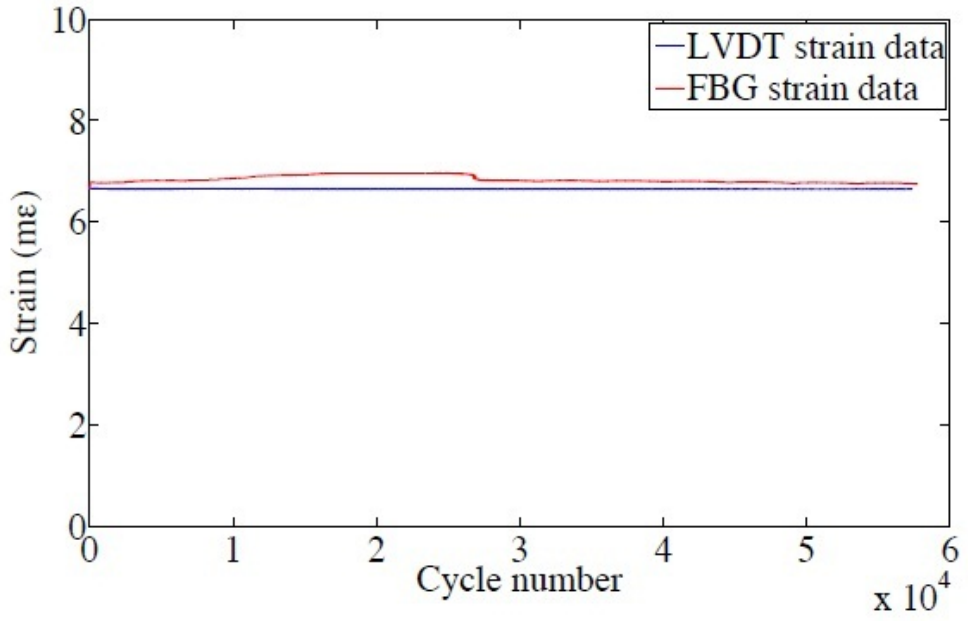

FIGURE 5.10: Strain data for Specimen 4-2

splitting phenomenon that results in an inaccurate strain level as shown in Figure 5.7.

The strain data calculated from the FBG sensor of Specimen 3-1 did not follow the displacement data from the LVDT. This was due to the uneven strain field occurred on the FBG sensor which broadened the reflected spectrum and split into two peaks. Existence of two peaks caused the interrogator to record wrong wavelength data which gave inaccurate strain values. The fatigue testing of Specimen 3-1 was performed for $\varepsilon_{max}/\varepsilon_{ult} = 0.5$ ratio. In order to eliminate spectrum broadenning and peak splitting, fatigue test of Specimen 4-2 was performed for $\varepsilon_{max}/\varepsilon_{ult} = 0.4$ ratio. The results of this specimen was better than the previous specimen. The prediction of the reamining life with FBG data was close to the prediction of the remaining life with LVDT data as seen in Figure 5.11. In real life applications, safety factor is generally more than 2 which ensures that composite materials are under strain levels less than $0.5^{*}\varepsilon_{max}$.

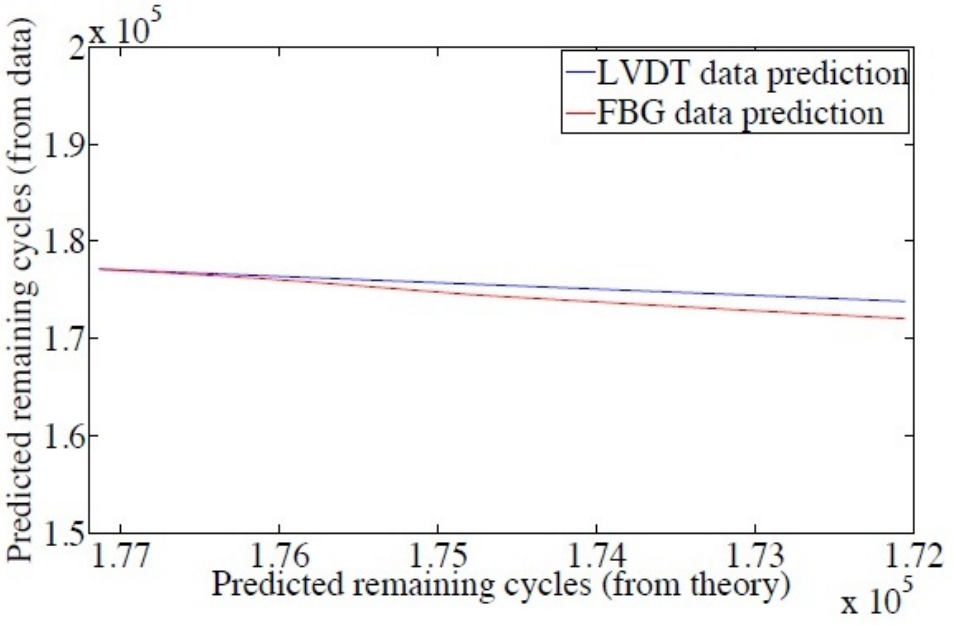

FIGURE 5.11: Prediction of remaining cycles for Specimen 4-2

However, to prove the effectiveness of the embedded FBG sensors in fatigue monitoring of composite materials similar fatigue monitoring for carbon fiber composites is proposed. Carbon fiber composites have usually lower ultimate tensile strain value than the maximum strain that embedded FBG sensor can sense.

5.5 Fatigue monitoring of carbon fiber composites

Considering the problems faced in fatigue monitoring of glass fiber composites, the carbon fiber composites are manufactured to have lower ultimate tensile strain value. FBG sensors used in previous section was $10mm$ long which increases the chance of peak splitting. Therefore $2mm$ long FBG sensors were embedded inside the carbon fiber composites.

5.5.1 Specimen preparation

The RTM apparatus in our lab which was described in Chapter 3 is modified to produce flat panels $610mm$ x $305mm$ x $1.7mm$ that are processed into specimens for fatigue testing.

The laminate selected for this research is $[0/90]_{2S}$ carbon fiber with epoxy resin. The fiber used is Chomarat 0/90 biaxial Woven Carbon Fabric with $380gsm$. The selected resin is Araldite LY 564 epoxy resin with XB 3403 hardener produced by Huntsman Corporation. The panels undergo an initial cure at $65°C$ for 24 hours with a post cure at $80°C$ for 24 hours. Six panels were produced for this study and processed into specimens. Specimens were named with the convention T#-##; with the first number indicating the panel they were cut from and second indicating the order in which they were cut. First three panel were used for preliminary investigation.

Each panel produces $\sim$25 specimens. Instead of using a tabbing material for the gripping area, the gripping area of the special fixture used in fatigue tests of glass fiber composites was modified. Channels in $1mm$ size were created on the surface of the fixture. Channels were used to constitute a diamond shape roughened surface similar to the grips of the MTS fatigue machine. This type of surface did not harm the specimen and holds the specimen tightly.

5.5.2 Material characterization test results

Ultimate tensile strain, ε_{ult}, is determined by 7 static tests. The ultimate stress and strain were found to be $500MPa$ and $6.69m\varepsilon$. The minimum stress applied to the specimen during fatigue testing is chosen first as $50MPa$ which is close to that used by Natarajan [47]. However, towards the end of the fatigue testing at 0.7 strain level minimum load has shown negative force values which contradicts tensile-tensile testing. The reason behind the crossing to the compression mode was that minimum displacement value was too low for the precision of the LVDT.

$\varepsilon_{max}/\varepsilon_{ult}$:	Energy Release Rate (J/cycle):	$r = U_f/U_0$:
0.7	6.06E-08	0.885
0.8	5.55E-05	0.934

TABLE 5.3: Fatigue test data for carbon fiber composites

Hence the minimum stress value is increased to $150MPa$ to ensure that minimum load does not cross to the negative values at any strain level.

After determining the ultimate stress and strain values, fatigue testing of the composite materials was carried out at 0.8 and 0.7 strain ratios so far. From the load data, expended strain energy per cycle is calculated and plotted. The plot of an expended strain energy per cycle was represented in Figure 5.12 which shows the same behavior in in Figure 2.7 as expected.

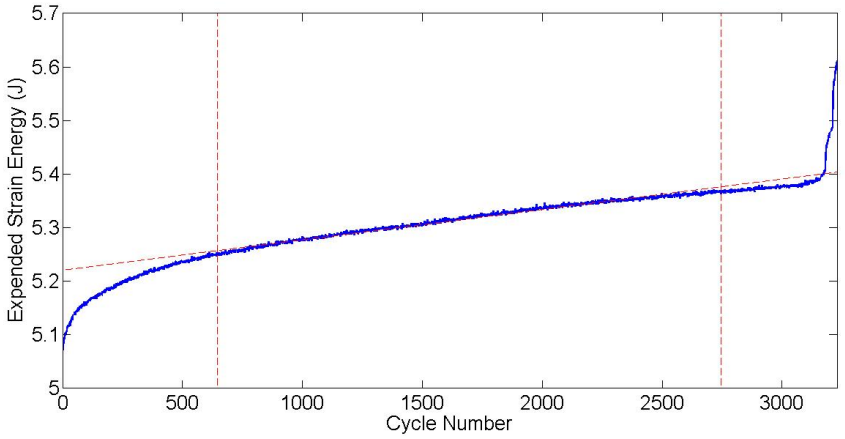

FIGURE 5.12: Expended strain energy per cycle for 0.8 strain ratio for carbon fiber composite specimen

Linear regression was used to obtain the energy release rate (dU/dN) throughout the linear region. The average energy release rate and ratio of U_f/U_0 for 0.8 and 0.7 of induced strain are presented in Table 5.3.

5.5.3 Remarks

Quasi-static tests of carbon fiber composites indicated that the ultimate tensile strain is below the maximum ultimate tensile strain of the embedded FBG sensors.

This ensures that fatigue testing of specimens with embedded FBG sensors can be performed for strain levels more than 0.4 ratio. The results of the 0.8 and 0.7 strain ratio fatigue tests agree with the fatigue test results of the glass fiber composites.

The fatigue tests of carbon fiber composites could not be completed in the duration of this thesis due to limited time. Therefore only static tests and fatigue tests for 0.8 and 0.7 strain ratios were performed for specimens without FBG sensors. The results promise that specimens with FBG sensor will deliver better results with regards to the prediction of the remaining useful life of the composite material.

Chapter 6

Conclusion

Overall objective of our group is to evaluate practicality and the feasibility of fiber optic based sensors for monitoring the state or the structural health of the composite materials from cradle to grave continuously, or from manufacturing phase to service phase. This thesis work was a continuation of the early works to achieve this objective.

At first the RTM apparatus in our lab was modified to manufacture 3D composite panels. This modification extended our capabilities of manufacturing composite panels with different sizes and different materials. FBG sensors were embedded into the composite structures during the manufacture process and these sensors have been utilized for cure and flow monitoring of the resin. In addition to the FBG sensors written on a single mode fiber optic cable, the abilities and worthiness of FBG sensors written on a polarization maintaining (PM) fiber optic cable was investigated in order to measure transversal strain besides longitudinal strain. It was observed that the load sensitivity of the PM FBG sensors is heavily dependent on the loading angle and in real applications, the angle of rotation of the sensor cannot be controlled pricesly and repeatedly. In conclusion, FBG sensors written on a PM fiber optic cable were not embedded into the composite materials.

In addition to process monitoring of composite structures, damage detection in composite structures was investigated with embedded FBG sensors. Embedded

FBG sensors were able to detect the presence of the artificial damage in the cantilever beam experiments. Ability of damage detection makes the embedded FBG sensors a good candidate for detecting fatigue induced damage and prediction of remaining useful life. In the extent of the investigation of ability of embedded FBG sensors for the prediction of remaining useful life has been performed via fatigue testing of glass and carbon fiber reinforced composites namely GFRC and CFRC. Eqs. 2.23 and 2.24 was added to the fatigue life prediction technique developed by Natarajan [47] allow for a stepwise addition of expended energy. This is a novel approach to remaining useful life prediction that allows a prediction to be made at each cycle. Although there were some problems regarding the limits of the FBG sensors, the fatigue experiments verified our novel approach to RUL prediction. To overcome the problems occurred with GFRC specimens, fatigue testing of CFRC was planned and started. However the testing has not been completed due to lack of time.

The results outlined in this thesis indicate that all three goals set in Chapter 1 have been accomplished. This study is an example of an interdisciplinary research which covers mechanical design and manufacturing, application of fiber optic sensors, fatigue modeling and signal processing.

The first work that should be done in the future is completion of fatigue testing of carbon fiber composite specimens and strain energy release rate per cycle for every strain ratio should be plotted and the unknowns a and b should be calculated. Subsequently, specimens with embedded FBG sensors should undergo fatigue testing at different strain ratios to prove their ability to predict the remaining useful life completely. Furthermore, this fatigue testing should be applied to different composite materials with different fiber orientations.

Bibliography

[1] S. H. Ahn, W. I. Lee, and G. S. Springer. Measurement of the three-dimensional permeability of fiber preforms using embedded fiber optic sensors. *Journal of Composite Materials*, 29(6):714–733, Apr. 1995.

[2] V. Antonucci, M. Giardano, L. Nicolais, A. Calabro, A. Cusano, A. Cutolo, and S. Inserra. Resin flow monitoring in resin film infusion process. In *Journal of Materials Processing Technology*, pages 687–692. CNR, Inst Composite Mat Technol, Dept Mat & Prod Engn, I-80125 Naples, Italy, 2003.

[3] G. Bektas, B. T., K. C.J., M. Yildiz, C. Ozturk, Y. Menceloglu, and A. Suleman. Fiber bragg grating and etched optic sensors for flow and cure monitoring of resin transfer molded composite structures. In *Proceedings of 18th International Conference on Composite Materials*, Jeju, South Korea, 2011.

[4] J. Bernstein and J. Wagner. Fiber optic sensors for use in monitoring flow front in vacuum resin transfer molding processes. *Review of Scientific Instruments*, 68(5):2156–2157, 1997.

[5] T. Boz, P. Chelliah, G. Bektas, F. Melemez, M. Yildiz, and C. Ozturk. Damage detection in composte plates using fiber bragg gratings. In *Proceedings of 15th European Conference on Composite Materials*, Venice, Italy, 2012.

[6] A. Bur, F. Wang, and C. Thomas. In-line optical monitoring of polymer injection molding. *Polymer Engineering and Science*, 34:671–9, 1994.

[7] F. Colpo, L. Humbert, and J. Botsis. Characterisation of residual stresses in a single fibre composite with fbg sensor. *Composites Science and Technology*, 67:1830–41, 2007.

[8] P. Crosby, G. Powell, G. Fernando, C. France, R. Spooncer, and D. Waters. In situ cure monitoring of epoxy resins using optical fibre sensors. *Smart Materials and Structures*, 5(4):415–428, 1996.

[9] A. Cusano, G. Breglio, M. Giardano, A. Calabro, A. Cutolo, and L. Nicolais. An optoelectronic sensor for cure monitoring in thermoset-based composites. *Sensors and Actuators a-Physical*, 84(3):270–275, 2000.

[10] W. Dang and N.-H. Sung. In-situ cure monitoring of diamine cured epoxy by fiberoptic fluorimetry using extrinsic reactive fluorophore. *Polymer Engineering and Science*, 34(9):707–715, May 1994.

[11] A. Davis. Study of an opto-ultrasonic technique for cure monitoring. In *Fiber Optic Smart Structures and Skins IV*, pages 264–274. SPIE, 1991.

[12] J. Degrieck and W. Van Paepegem. Fatigue damage modeling of fibre-reinforced composite materials: Review. *Applied Mechanics Reviews*, 54(4):279, 2001.

[13] C. Dennison and P. Wild. Enhanced sensitivity of an in-fibre Bragg grating pressure sensor achieved through fibre diameter reduction. *Measurement Science and Technology*, 19, Oct. 2008.

[14] C. R. Dennison and P. M. Wild. Sensitivity of bragg gratings in birefringent optical fibre to transverse compression between conforming materials. *Applied Optics*, 49(12):2250–61, 2010.

[15] C. R. S. Dennison. *Development of in-fibre Bragg grating contact force sensors for application to the human hip.* PhD thesis, University of Victoria, 2011.

[16] V. Dewynter-Marty, P. Ferdinand, E. Bocherens, R. Carbone, H. Beranger, S. Bourasseau, M. Dupont, and D. Balageas. Embedded fiber Bragg grating sensors for industrial composite cure monitoring. *Journal of Intelligent Material Systems and Structures*, 9(10):785–787, 1998.

[17] C. Doyle, A. Martin, T. Liu, and M. Wu. In-situ process and condition monitoring of advanced fibre-reinforced composite materials using optical fibre sensors. *Smart materials and Structures*, 7(2):145, 1998.

[18] G. Duan, V. Lyori, and M. R. Bragg grating fiber applied in strain measurement. In *Proceeding of The 2nd Annual Symposium On Computer Science and Electrical Engineering*, Lulea, Sweden, 2001.

[19] J. Dunkers, J. Lenhart, and S. Kueh. Fiber optic flow and cure sensing for liquid composite molding. *Optics and lasers in Engineering*, 35(2):91–104, 2001.

[20] J. R. Dunphy. Multifunction, distributed optical fiber sensor for composite cure and response monitoring. In *Fiber Optic Smart Structures and Skins III*, pages 116–118. SPIE, Dec. 1990.

[21] S. Eum, K. Kageyama, H. Murayama, I. Ohsawa, K. Uzawa, M. Kanai, and H. Igawa. Resin flow monitoring in vacuum-assisted resin transfer molding using optical fiber distributed sensor. In *Proceedings of SPIE*, pages 65262T–65262T–8. SPIE, Apr. 2007.

[22] G. Fernando, T. Liu, P. Crosby, C. Doyle, A. Martin, D. Brooks, B. Ralph, and R. Badcock. A multi-purpose optical fibre sensor design for fibre reinforced composite materials. *Measurement Science and Technology*, 8(10):1065–1079, 1997.

[23] N. Gupta and R. Sundaram. Fiber optic sensors for monitoring flow in vacuum enhanced resin infusion technology (VERITy) process. *Composites Part A: Applied Science and Manufacturing*, 40(8):1065–1070, 2009.

[24] B. Harris, editor. *Fatigue in composites*. Woodhead Publishing, 2003.

[25] J. Hecht. *Understanding fiber optics*. Pearson Education Inc., Upper Saddle River, New Jersey, 2006.

[26] K. O. Hill, Y. Fujii, D. C. Johnson, and B. S. Kawasaki. Photosensitivity in optical fiber waveguides: application to reflection filter fabrication. *Applied Physics Letters*, 32(10):647–649, 1978.

[27] W. Hwang. Fatigue of composites—fatigue modulus concept and life prediction. *Journal of Composite Materials*, 1986.

[28] W. Hwang and K. Han. Cumulative Damage Models and Multi-Stress Fatigue Life Prediction. *Journal of Composite Materials*, 20(2):125–153, 1986.

[29] S. James, M. Dockney, and R. Tatam. Simultaneous independent temperature and strain measurement using in-fibre Bragg grating sensors. *Electronics Letters*, 32(12):1133–1134, 1996.

[30] J.Botsis, L.Humbert, F.Colpo, and P.Giaccari. Embedded fiber bragg grating sensor for internal strain measurements in polymeric materials. *Optics and Lasers in Engineering*, 43:491–510, 2005.

[31] K. Jung and T. Jin Kang. Cure Monitoring and Internal Strain Measurement of 3-D Hybrid Braided Composites using Fiber Bragg Grating Sensor. *Journal of Composite Materials*, 41(12):1499–1519, June 2007.

[32] C. Keulen, F. Melemez, T. Boz, P. Chelliah, H. Turkmen, M. Yildiz, and A. Suleman. Prediction of fatigue response of composite structures by monitoring the strain energy release rate with embedded fiber bragg gratings. *Journal of Intelligent Material Systems and Structures*, submitted, 2012.

[33] C. Keulen, M. Yildiz, and A. Suleman. Multiplexed FBG and Etched Fiber Sensors for Process and Health Monitoring of 2-&3-D RTM Components. *Journal of Reinforced Plastics and Composites*, 30(12):1055–1064, 2011.

[34] K. Kuang. Use of conventional optical fibers and fiber Bragg gratings for damage detection in advanced composite structures: a review. *Applied Mechanics Reviews*, 2003.

[35] C. M. Lawrence, D. V. Nelson, E. Udd, and T. Bennett. A fiber optic sensor for transverse strain measurement. *Experimental Mechanics*, 39:202–209, 1999.

[36] J.-R. Lee and H. Tsuda. Acousto-ultrasonic sensing using capsular fibre Bragg gratings for temperature compensation. *Measurement Science and Technology*, 17(11):2920–2926, Oct. 2006.

[37] L. Lee, K. Fu, and J. Yang. Prediction of fatigue damage and life for composite laminates under service loading spectra. *Composites Science and Technology*, 56(6):635–648, 1996.

[38] S. T. Lim and W. Lee. An analysis of the three-dimensional resin-transfer mold filling process. *Composites Science and Technology*, pages 961–975, 2000.

[39] H. F. Lima, P. F. Antunes, J. d. L. Pinto, and R. N. Nogueira. Simultaneous Measurement of Strain and Temperature With a Single Fiber Bragg Grating Written in a Tapered Optical Fiber. *Ieee Sensors Journal*, 10(2):269–273, 2010.

[40] G. Luyckx, L. Voet, N. Lammens, and J. Degrieck. Strain measurements of composite laminates with embedded fibre bragg gratings: Criticism and opportunities for research. *Sensors*, 11:384–408, 2011.

[41] R. E. Lyon, K. E. Chike, and S. M. Angel. In situ cure monitoring of epoxy resins using fiber-optic Raman spectroscopy. *Journal of Applied Polymer Science*, 53(13):1805–1812, Sept. 1994.

[42] J. Maguire and P. Talley. Remote Raman-Spectroscopy as a Sensor Technology in Composite-Materials Processing. *Journal of Advanced Materials*, 26(2):27–40, 1995.

[43] D. Marcuse. *Light Transmission Optics*. Nostrand Reinhold Company Inc, New York, N.Y., 1982.

[44] R. Measures. *Structural Monitoring with Fiber Optic Technology*. Academic Press, San Diego, 2001.

[45] V. Murukeshan, P. Chan, L. Ong, and L. Seah. Cure monitoring of smart composites using Fiber Bragg Grating based embedded sensors. *Sensors and Actuators a-Physical*, 79(2):153–161, 2000.

[46] M. L. Myrick, S. M. Angel, R. E. Lyon, and T. M. Vess. Epoxy cure monitoring using fiber-optic Raman spectroscopy. *SAMPE Journal*, 28:37–42, Aug. 1992.

[47] V. Natarajan and H. Gangarao. Fatigue response of fabric-reinforced polymeric composites. *Journal of Composite Materials*, 2005.

[48] R. Neff and D. Woerdeman. Use of a charged coupled device (CCD) camera for evanescent wave optical fiber cure monitoring of liquid composite molding resins - Neff - 2004 - Polymer Composites - Wiley Online Library. *Polymer composites*, 1997.

[49] Y. Okabe, T. Mizutani, S. Yashiro, and N. Takeda. Detection of microscopic damages in composite laminates : with embedded small-diameter fiber Bragg grating sensors. *Composites Science and Technolo*, 62(7-8):951–8, 2002.

[50] Y. Okabe, R. Tsuji, and N. Takeda. Application of chirped fiber Bragg grating sensors for identification of crack locations in composites. *Composites Part A: Applied Science and Manufacturing*, 35(1):59–65, 2004.

[51] Y. Okabe, S. Yashiro, T. Kosaka, and N. Takeda. Detection of transverse cracks in CFRP composites using embedded fiber Bragg grating sensors. *Smart Materials and Structures*, 9(6):832–838, 2000.

[52] A. Othonos and K. Kalli. Fiber Bragg gratings: fundamentals and applications in telecommunications and sensing. Artech House, Inc., 1999.

[53] N. G. Ozdemir. Process monitoring of resin transfer molded composite structures by fiber optic sensors. Master's thesis, Sabanci University, Istanbul, 2011.

[54] H. Paik. Fiberoptic intrinsic fluorescence for in-situ cure monitoring of amine cured epoxy and composites. *Polymer Engineering and Science*, 1994.

[55] H. Patrick, G. Williams, A. Kersey, J. Pedrazzani, and A. Vengsarkar. Hybrid fiber bragg grating/long period fiber grating sensor for strain/temperature discrimination. *Photonics Technology Letters, IEEE*, 8:1223 –1225, 1996.

[56] S. Roberts. Cure and fabrication monitoring of composite materials with fibre-optic sensors. *Composites Science and Technology*, 1993.

[57] A. Rotem. A Fatigue Failure Criterion for Fiber Reinforced Materials. *Journal of Composite Materials*, 1973.

[58] S. Schwab. Monitoring the composite curing process with a fluorescence-based fiber-optic sensor - Levy - 2004 - Polymer Composites - Wiley Online Library. *Polymer composites*, 1991.

[59] C. Shin. Fatigue damage monitoring in polymeric composites using multiple fiber Bragg gratings. *International journal of fatigue*, 2006.

[60] N. Takeda. Characterization of microscopic damage in composite laminates and real-time monitoring by embedded optical fiber sensors. *International journal of fatigue*, 2002.

[61] N. Takeda, S. Yashiro, and T. Okabe. Estimation of the damage patterns in notched laminates with embedded FBG sensors. *Composites Science and Technology*, 66(5):684–693, May 2006.

[62] S. Takeda, Y. Okabe, and N. Takeda. Delamination detection in CFRP laminates with embedded small-diameter fiber Bragg grating sensors. *Composites Part A: Applied Science and Manufacturing*, 33(7):971–980, July 2002.

[63] G. Thursby, B. Culshaw, and D. C. Betz. Multifunctional fibre optic sensors monitoring strain and ultrasound. *Fatigue & Fracture of Engineering Materials & Structures*, 31(8):660–673, Aug. 2008.

[64] S. W. Tsai, S. Ha, T. E. Tay, Y. Miyano, and S. Sihn. *Strength & Life of Composites*. Aero & Astro, Stanford U, 2008.

[65] E. Udd. *Fiber optic smart structures*. John Wiley & Sons, Inc., New York, 1995.

[66] E. Udd and W. Schulz. Multiaxis fiber grating strain sensor applications for structural monitoring and process control. In *Proceedings of SPIE*, 1999.

[67] H. Whitworth. A stiffness degradation model for composite laminates under fatigue loading. *Composite structures*, 1997.

[68] H. A. Whitworth. Modeling Stiffness Reduction of Graphite/Epoxy Composite Laminates. *Journal of Composite Materials*, 21(4):362–372, Jan. 1987.

[69] H. A. Whitworth. Cumulative Damage in Composites. *Journal of Engineering Materials and Technology*, 112(3):358, 1990.

[70] D. Woerdeman, J. Spoerre, and K. Flynn. Cure monitoring of the liquid composite molding process using fiber optic sensors . *Polymer Composites*, 18(1):133–150, 1997.

[71] M. Xu, J. Archambault, L. Reekie, and J. P. Dakin. Discrimination Between Strain and Temperature Effects Using Dual-Wavelength Fiber Grating Sensors. *Electronics Letters*, 30(13):1085–1087, 1994.

[72] J. Yang, D. Jones, and S. Yang. A stiffness degradation model for graphite/epoxy laminates. *Journal of Composite Materials*, 24(7):753–769, 1990.

[73] S. Yashiro and T. Okabe. Estimation of fatigue damage in holed composite laminates using an embedded FBG sensor. *Composites Part A: Applied Science and Manufacturing*, 42:1962–9, 2011.

[74] C. Ye, S. E. Staines, S. W. James, and R. P. Tatam. A polarization-maintaining fibre bragg grating interrogation system for multi-axis strain sensing. *Measurement Science and Technology*, 13:1446–9, 2002.

[75] M. Yildiz, N. Ozdemir, G. Bektas, C. Keulen, T. Boz, E. Sengun, C. Ozturk, Y. Menceloglu, and A. Suleman. An experimental study on the process monitoring of resin transfer molded composite structures using fiber optic sensors. *ASME- Journal of Manufacturing Science and Engineering*, 134(4):044502, 2012.